Circulation Redistribution in Leading-edge Vortices on Rotating Wings

by

Clara Giner-Morency

A thesis submitted in partial fulfillment of the requirements for the degree of

Master of Science

Department of Mechanical Engineering
University of Alberta

Abstract

This work presents an investigation into the circulation transport within a leading-edge vortex (LEV) on a rotating wing and its governing dynamics. These dynamics were used to produce a model for the computationally inexpensive prediction of circulation growth and distribution within an LEV. The test-case used in this study was performed on a thin flat plate in rotation at Reynolds numbers (Re) of $Re = 1000$ and $Re = 2500$.

The model conceptualizes the circulation transport as species transport, which means that fluid particles entering the leading-edge vortex shear-layer are conceptualized as vorticity-containing mass and are advected perfectly by the spanwise flow. The present work thus offers a study of the extent to which circulation is tied to mass, for some classes of three-dimensional flows. From the vorticity transport equation, a circulation balance is developed between a proposed circulation generation and the vorticity transport terms, such that only two unknows must be characterized by the model itself: the shear-layer velocity profile and the spanwise flow distribution. A shear-layer velocity relationship with the mass rate entering the LEV is suggested such that the modeller only needs to determine the shear-layer thickness. The spanwise flow distribution is characterized by a Bernoulli-derived equation such that both the rotational acceleration and the pressure gradient along the span are represented.

To verify the validity of the concept and the accuracy of the model predictions, the model is compared against experimental circulation measurements taken with particle image velocimetry (PIV) and show good agreement given an accurate spanwise flow. Moreover, the validity of both the shear-layer velocity profile model and the spanwise flow distribution approximation is investigated individually, again against experimental measurements. While

the model showed sensitivity to the spanwise flow, the model showed to be insensitive to the value chosen by the modeller for the shear-layer thickness (the only unknown parameter).

Lastly, the present work offers an investigation of the vorticity annihilation and its effect on the modelled net circulation. The present work suggests that vorticity annihilation may be a local property and that the net circulation in the near-field of a wing may be determined from the leading-edge shear-layer alone. Hence, the present work argues that modelling the net circulation accounts for the vorticity annihilation mechanism acting locally without having to model the extra term.

Preface

The present thesis is presented as a compilation of two articles. Central chapters consist of multi-authored work in the form of articles. As the experimental methodology and concept from both articles overlap, the contributions are presented in a similar manner. The experimental data is shared between the two articles, but they constitute significantly different analysis and conceptual contributions. The contribution of each co-author is presented below:

Chapter 2, "A species-transport model for circulation in a leading-edge vortex" has been submitted to *Advances in Aerodynamics* and currently the manuscript is awaiting revision from the first round of reviews.

Chapter 3,"Modelling Circulation Growth in Leading-edge Vortices" is currently under revisions.

I developed the methodology, conducted the experiments presented in this article and completed the experimental data analysis, all under the supervision of Dr. Wong. The project was initially conceptualized by Dr. Wong and I implemented the model concepts into a computational script. The text of the above manuscripts were produced by me. Dr. Wong reviewed and edited drafts of the text.

The content of both Chapter 2 and 3 is presented as submitted to the journal, with the only exception that the symbols have been standardized between the two articles to facilitate the readability of this thesis. The format and citation style were also altered to follow the structure requirements of this thesis.

As both articles are awaiting publication at this moment, the copyright is shared equally between co-authors.

Acknowledgements

I would first like to thank my supervisor Dr. Jaime G. Wong from the Mechanical Engineering Faculty at University of Alberta. The door to Prof. Wong office was always open for in-person or virtual meetings whenever I faced a difficulty or had questions about my research or writing. He showed support during the unpredictable turn my studies took due to the pandemic. He consistently allowed this paper to be my own work, but steered me in the right direction for success.

I would also like to thank my supervisory committee Dr. Alexandra Komrakova and Dr. Carlos Lange from the Mechanical Engineering at University of Alberta.

J'aimerais remercier du fond du coeur ma famille qui m'a offert un support inconditionel en m'encourageant tout au long de mes études et sans qui cet accomplissement n'aurait pas été possible. J'aimerais remercier particulièrement mon père qui m'a accompagnée dans mes réussites et dans mes échecs sans jamais ne douter de ma place, et de celle des femmes, en sciences. Enfin, un merci tout spécial à mon chat Edgar qui m'a suivie dans mes aventures à l'autre bout du pays.

Contents

List of Figures

List of Symbols

Symbol	Definition	Units
c	wing's chord	(m)
b	wing's span	(m)
τ	wing's thickness	(m)
t	time	(s)
t^*	adimensional time	-
m	mass property	(kg)
m'	mass into the LEV per unit span	(kg/m)
d	shear layer thickness	(m)
l	shear layer length	(m)
A	vortex area	(m^2)
R_{LEV}	radius of the vortex area defined by the blockage	(m)
r_{LEV}	distance from the vortex center	(m)
$\vec{n}$	unit vector	-
x, y	fixed coordinates	(m)
z	spanwise position from the axis of rotation	(m)
z^*	adimensional spanwise position	-
z_0	radial position of the root of the wing	(m)
Z_T	radial position of wing tip	(m)
Z	span domain	-
i	discritized bins along the span	-
N	particles contained in each bin	-
u, v	x- and y- velocity components	(m/s)
w	spanwise flow velocity	(m/s)
$\overline{w}$	average spanwise flow velocity	(m/s)
w_0	local spanwise flow velocity at the root	(m/s)
$\vec{u}$	velocity vector	(m/s)
$\vec{u_{\text{eff}}}$	local flow velocity vector	(m/s)
U_T	flow velocity evaluated at the wing tip	(m/s)
U_∞	free stream velocity	(m/s)
U	shear-layer velocity	(m/s)
u_o	outer shear-layer velocity	(m/s)
u_i	inner shear-layer velocity	(m/s)
u_{eff}	effective shear layer velocity	(m/s)

Symbol	Definition	Units
P	pressure	(Pa)
g	gravitationnal acceleration	(N)
k	constant of proportionality or particle subscript for local properties	-
C_{ps}	base pressure coefficient	-
Δ	interval	-
Γ	circulation	-
Γ^*	adimensional circulation	-
Γ_{net}	net circulation over the entire LEV region	-
Γ_1	circulation of the primary LEV vortex	-
Γ_2	circulation of the secondary LEV vortices	-
ρ	density	(kg/m^3)
μ	dynamic viscosity	$(kg/m \cdot s)$
ν	kinematic viscosity	(m^2/s)
θ	angle of revolution completed by the wing	(rad)
Ω	rotational speed	(rad/s)
ω	vorticity	(m/s)
$\vec{\omega}$	vorticity vector	(m/s)
∇	divergence	-
η	shear layer coordinate	-
α	angle of attack	(deg)
α_{eff}	angle formed by local and free stream velocities	(deg)
δ	boundary layer thickness	(m)

Glossary

aspect ratio (AR)

aspect ratio of the wing AR = b/c

leading-edge suction parameter (LESP)

leading-edge vortex (LEV)

micro-air vehicles (MAV)

particle image velocimetry (PIV)

Particle image velocimetry is used to obtain the experimental measurements to characterize the flow

Reynolds numbers (*Re*)

Reynolds number defined at the wing tip

unmanned aerial vehicles (UAV)

Chapter 1

Introduction

While birds have been of great inspiration for man-made flight, knowledge of their flight mechanics is still limited and, while engineered flyers are relatively well-understood, their performance is not yet comparable to biological flight at small scales and low speeds. Bio-inspired and bio-engineered flight are therefore of keen interest with the advent of smaller-scale unmanned aerial vehicles (UAV), which explains the recent increase in interest taken to investigate and characterize biological flight. For instance, Dial (1992); Tobalske and Dial (1996); Tobalske et al. (2004) studies on wing kinematics lead to engineering research to take place into bio-inspired flights. Later, Tobalske (2007) presented a study of the biomechanics during a bird flight, showing with precision how birds control their flight performances continuously, adapting rapidly to transient flow conditions. Carruthers et al. (2007, 2010) and Berg and Biewener (2010), just to name a few, have investigated the kinematics and the dynamics of the most unsteady phases of bird flight, which are the take-off and perching. However, the kinematics of wing motion only translate to force via the fluid mechanics surrounding the bird or flyer. One of the challenges of bio-inspired and bio-engineered flight research and development from a fluid mechanic perspective is that it requires us to study complex highly three-dimensional flow phenomenon, resultant from flapping wings, such as leading-edge vortices (LEVs).

LEVs forms on wings when positioned at high angle-of-attack α, when the angle-of-attack is increased rapidly or when spanwise flow is present, which all result in a dynamic stall.

Under these conditions, the flow separates from the wing profile at the leading-edge and forms a vortex. The LEV primary vortex itself will then induce along the wing surface, by entrainment, weaker secondary vortices opposite in sign to the LEV, as shown in Figure 1.1. Those interactions between the primary and secondary vortices affect the local vorticity dynamics and are referred to as vorticity annihilation mechanism. Among the properties of LEVs we wish to characterize is the so-called stable LEV, characterized by a constant position and strength, which implies that the influx of vorticity into the LEV must balance the vorticity transported out. By way of comparison, classical stall results in a drastic lift drop, whereas dynamic stall generated by LEVs results in significant lift enhancement prior to vortex detachment (see: Rival et al., 2014). This lift increase explains why flyers have been observed to morph their wings or shift their body shape rapidly, resulting in a dynamic stall, when perching.

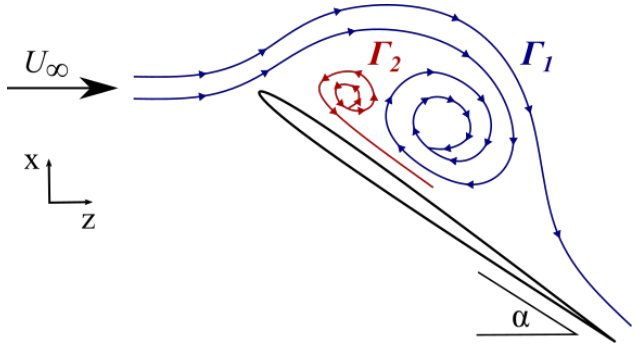

Figure 1.1: Leading-edge vortex forming on a wing positioned at an angle-of-attack α maintained under a constant free stream velocity U_∞. The flow separates at the leading-edge and forms a primary vortex (represented in blue), which results in opposite-sign secondary vortices creation at the surface of the wing (represented in red). Vorticity and circulation generated within the shear-layer is fed into the vortex and defines its strength. Circulation is transported along the span with spanwise flow through the LEV, until it joins tip vortices. Vortex grows until it detaches from the wing.

LEVs present flow behaviours complex to describe due to highly three-dimensional flow characteristics, such as the transport of circulation by spanwise flow. However, understanding their dynamics is essential for the design of micro-air vehicles (MAV) or UAVs, as researchers have observed that the LEV on a flapping wing is one of the high lift mechanisms critical for both lift generation and flight control (see: Ellington et al., 1996; Birch et al., 2004).

The stability of an LEV and its critical parameters are still the subject of investigation (see: Jones and Babinsky, 2011; Jones et al., 2011) and the underlying mechanism of LEV stability remains the subject of debate. For instance, Lentink and Dickinson (2009a,b) demonstrated that the stability of an LEV can be characterized by its aspect ratio (AR). Assuming a stable LEV can be identified, investigations can be made to describe the LEV growth and development, which itself relies on a better understanding of vorticity transport. The work of Rival showed the importance to investigate and predict the LEV circulation growth and detachment, and the benefits it has on the bio-inspired and bio-engineered research fields (see: Rival et al., 2010; Rival and Tropea, 2010; Rival et al., 2014). LEV parameters, such as its strength and its location, are obviously affected by the vorticity dynamics, which are thought to be the direct cause of LEV stability. Therefore, effective models for vorticity or circulation growth in LEVs not only lead to improved force prediction such as pressure or lift, but also gives tremendous physical insights into the LEV formation process itself and about the flow behaviours from a vorticity transport perspective.

1.1 Objectives of the Present Work

Most models for circulation growth only consider the two-dimensional problem of circulation entering an LEV but don't characterize the transport through spanwise convection. For example, Polhamus (1966) developed a leading-edge suction model from thin airfoil theory that was later developed by Ramesh et al. (2014, 2018) into two-dimensional point vortex models for LEV growth. The available models are not adapted for highly three-dimensional flows, such as those on rotating wings, as circulation growth models must consider both generation and transport terms. The present work, presented as two research chapters, aims to model circulation growth for a rotating wing, inspired from model concepts originally developed and validated for translating delta wings, where spanwise flow is constant.

The present work aims to offer an effective yet computationally inexpensive model as a solution to predict circulation distribution within the LEV of a rotating wing and to provide physical insight into the circulation transport process. To achieve this goal, the present work

will define the circulation generation and the circulation transport for the specific case of a rotating wing. Moreover, from the simplified version of the vorticity transport equation that we will derive, we wish to gain insights on the fluid dynamics describing the flow within an LEV on a rotating wing. The suggested circulation model aims to define the role and the effects of each term characterizing the vorticity transport equation, such as vortex tilting and stretching and viscous diffusion, on the circulation generation and transport itself. Additionally, the modelling exercise aims to define the role of vorticity annihilation when computing the net circulation.

To achieve our general goal of modelling the circulation distribution for an LEV on a rotating wing, the modelling efforts will be compared to experimental circulation values obtained from a rotating wing at a fixed angle-of-attack submerged in a 1 m^3 tank filled with water, as shown in Figure 1.2. The wing is maintained at a constant rotational speed Ω. The experimental measurements to characterize the flow behaviours are obtained with PIV and optical set-ups.

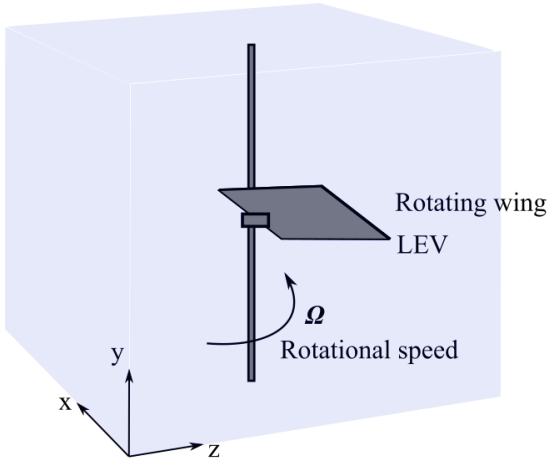

Figure 1.2: The rotating wing experimental test case is used to validate the model. The rotating wing is submerged into a water tank. Its rotational speed Ω is constant through the completion of specific revolution angle motion θ. The rotating wing presents a fixed angle-of-attack α.

In turn, this work will address four primary research questions, detailed in the following sections:

1. can we model the LEV dynamics with species transport;

2. can we accurately approximate the circulation generation within the LEV by the shear-layer velocity;

3. does an accurate model for net circulation require explicit accounting of vorticity annihilation term; and

4. what is the role of the pressure gradient term when modelling the spanwise flow distribution?

1.1.1 Species Transport

Mass and circulation transport are coupled but non-identical problems, as the vorticity transport equation shows that the substantial derivative of vorticity is non-zero (i.e. it is non-conservative). Traditionally, mass and circulation evaluation both require knowledge of the vorticity field. Interpreting the vorticity transport equation as species transport is a simplification initially suggested by Wong et al. (2013) to track mass and to track circulation on an LEV for a translating wing (see: Wong et al., 2018), but this is a very narrow scope. The fundamental concept of this model is to assume that circulation follows the mass in the flow, which implies that vorticity is conservative under certain conditions. The fluid particles are therefore particles representing vorticity-containing mass. The simplicity of the model offers computational efficiency. Each particle representing mass across the wing span is assigned simultaneously a mass and circulation based on the shear-layer properties, and is then allowed to advect along the span. The total mass or circulation at a spanwise location is the sum of that represented by all the particles at that location (both those just generated and those advected there). The species transport model considers a simplified vorticity transport equation for an incompressible fluid as its governing equation:

$$\frac{\partial \vec{\omega}}{\partial t} + (\vec{u} \cdot \nabla)\vec{\omega} = (\vec{\omega} \cdot \nabla)\vec{u} + \nu \nabla^2 \vec{\omega} = 0 \ . \tag{1.1}$$

The physical meaning for each term, from left to right, are described as the local vorticity change in the fluid due to unsteadiness, convection, vortex stretching and tilting due to velocity gradients and viscous diffusion of the vorticity. The simplification of the vorticity transport equation is achieved by the hypothesis that mass can be represented as conservative (under specific conditions), such that vorticity transport is strictly described by its substantial derivative. The vortex tilting and stretching term and the viscous diffusion term are implicitly assumed to be zero by defining them as following mass perfectly (i.e. vorticity-containing mass fluid particles). The model ignores the vortex tilting term under the assumption of flow far from the tip vorcities, where vortex tilting is significant. In the context of studying the transport of circulation along the span, rather than vorticity, the vortex stretching term is zero since circulation is conserved under vortex stretching (see: Wojcik and Buchholz, 2014). These hypotheses are supported by Cheng et al. (2013) as they showed that, under similar conditions, vortex tilting and stretching have a smaller effect than convection for a rotating wing. Even if some studies have shown the viscous term to be significant in the circulation balance in some circumstances (e.g., Wojcik and Buchholz, 2014), we will investigate the viscous effects again here, as the timescale difference between viscous diffusion and vortex growth might influence its role. Thus, if we were to integrate the vorticity transport equation to convert it into a circulation transport equation, we would expect only the convection term to remain to balance circulation fed into the control volume from the leading-edge shear layer. Therefore, assuming this circulation balance, the two terms left to define would be the vorticity generation rate and its transport through convection within the spanwise flow.

To verify the model concept and therefore the above assumptions, the circulation distribution predicted by the model must be compared against experimental circulation values obtained with PIV. Matching values would validate its core assumptions of negligible vortex tilting and stretching and confirm that the species transport accurately model the circulation distribution within an LEV on a rotating wing. Furthermore, the present work will target flow characterized by low Reynolds numbers to maximise the viscous effects, such that the

viscosity effect on the circulation can be evaluated. If the viscous diffusion is negligible, the circulation distribution will be insensitive to the Reynolds number variation. The validation of the species transport model would implicitly confirm the hypothesis that vorticity is a conservative property under the conditions prescribed above.

1.1.2 Vorticity Annihilation

As the present work aims to model circulation growth via circulation balance, it indirectly investigates the importance of modelling vorticity annihilation. Recent studies, such as Wojcik and Buchholz (2014), Medina and Jones (2016), Onoue and Breuer (2017) and as summarized by Eldredge and Jones (2019), have characterized vorticity annihilation as a critical mechanism in the above circulation balance, but it is still unclear if it must be included in a circulation modelling exercise, and if so under what conditions. While the vorticity annihilation concept in itself is uncontroversial, the present work aims to demonstrate that modelling circulation doesn't require an extra term to represent the vorticity annihilation since it may be accounted for inherently in control volume selection. This demonstration does not question the existence of the vorticity annihilation mechanism itself, but to what extent it is a fundamental part of modelling *net* LEV circulation.

Vorticity annihilation was identified as the entrainment of opposite-signed vorticity generated on the wing surface by the LEV (see: Onoue and Breuer, 2017). This identified region of opposite-signed vorticity affects the local vorticity dynamics, however the present work questions its effect on the net circulation, as the net circulation must match the large-scale shear of the flow. In a study investigating vorticity generation, Morton (1984) showed that the vorticity generation (and thus the resulting circulation), in a boundary layer of thickness δ on a flat plate maintained under free-stream velocity U_∞ happens entirely at the leading edge and is convected along the plate as shown in Figure 1.3 (adapted from Morton (1984) original study Figure 6). This specific study case, and every other case presented in that study, demonstrated that vorticity generation and destruction happens at boundaries, such that local variations in vorticity, like in a specific boundary layer profile, does not affect the

net circulation. That concept leads to the assumption that the LEV control volume selection can offer a good alternative to take account for the vorticity annihilation without having to model it.

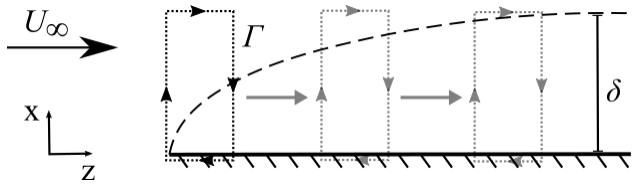

Figure 1.3: Vorticity, and thus the resulting circulation Γ, in a boundary layer on a flat plate of thickness δ are generated at the leading edge and convected along the plate through the flow generated by the free-stream velocity U_∞. While the vorticity annihilation has local effects on the flow, the net circulation of the control volume isn't affected by the internal fluctuations.

The suggested model aims to define the net circulation ($\Gamma_{\text{net}} = \Gamma_1 - \Gamma_2$ from Figure 1.1), rather than either the positive or the negative circulation regions, such that the selected control volume contains the entire LEV region (positive and negative vorticity generated by primary and secondary vortices). The control volume selection is presented in Figure 1.4. We hope to show that the vorticity annihilation, under these conditions, doesn't need to be modelled, while its local effects on the circulation are not ignored. As vorticity annihilation has been identified as a residual term computed from the circulation budget by previous studies (e.g., Wojcik and Buchholz, 2014; Medina and Jones, 2016), matching predicted circulation values with experimental circulation values will indicate that modelling net circulation is sufficient and accounts for the vorticity annihilation mechanism inherently.

1.1.3 The Shear-layer Velocity Profile

As stated as one of our main research questions, the present work attempts to describe the circulation generation in the leading-edge shear layer, upstream of an LEV, by a relationship with the leading-edge shear-layer velocity U:

$$\left(\frac{\partial \Gamma}{\partial t}\right)_{\text{in}} = \frac{1}{2}U^2 \ . \tag{1.2}$$

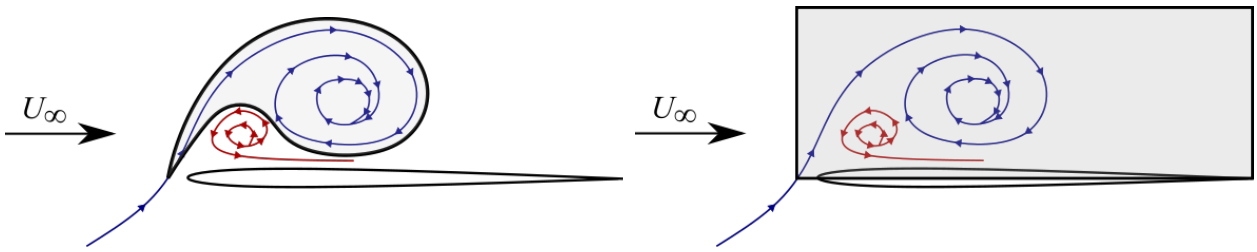

Figure 1.4: Control volume selection over the LEV region to compute (A) the total circulation of the primary vortex (B) the net circulation of the entire LEV region (both positive and negative vorticity from the primary and secondary vortices). In the case of modelling the circulation of the primary vortex strictly like presented in the left-side case, the vorticity annihilation must be accounted for.

The exact derivation is presented in Chapter 3, but it is worth noting that similar results, from distinct derivations, have been obtained for circulation generation within a shear-layer, a boundary layer and for piston-cylinder configurations (see: Wong et al., 2018; Morton, 1984; Didden, 1979). The present work expects the LEV on a rotating wing to be generated in the leading-edge shear-layer, such that the circulation generation can be described by Equation 1.2. To determine if the circulation influx into the LEV can be approximated in this way, the circulation flux across the shear-layer must be compared with the exact value. For a shear-layer velocity aligned with the free-stream velocity u, and thus assuming a small prependicular velocity component v, then vorticity is contained entirely in the term $\partial u/\partial y$. Therefore, vorticity is transported across the shear-layer by velocity as $u(\partial u/\partial y)$, and the exact value of circulation flux into the vortex is therefore the integral of this parameter across the shear-layer thickness. If the values match within a small difference tolerance, we would conclude that the circulation generation approximation is reasonable.

If the rate of circulation growth proves to be accurately evaluated with the shear-layer feeding relationship (Equation 1.2), and if the vorticity proves to be conservative following Section 1.1.1, the circulation could be represented as a balance of the circulation generation and spanwise transport. The rate at which circulation is removed from the vortex through spanwise convection is calculated by integrating the vorticity-transport equation over the vortex area. The circulation balance derived from the vorticity transport equation would be

then presented as:

$$\left(\frac{\partial \Gamma}{\partial t}\right)_{\text{in}} - \left(\frac{\partial \Gamma}{\partial t}\right)_{\text{out}} = \frac{1}{2}U^2 - \overline{w}\frac{\partial \Gamma}{\partial z} \ , \tag{1.3}$$

such that both the shear-layer velocity profile and the spanwise flow distribution must be modelled. The shear-layer velocity profile plays an important role in the circulation flux through the leading-edge shear-layer. Therefore, many studies investigating vortex growth have tried to model its distribution. For example, Roshko (1954) suggested a shear-layer velocity relationship with the free-stream velocity and the base-pressure coefficient. However, most of those available models are hardly adapted for a predictive model, as they present unknown parameter limitations. The study presented in Chapter 2 chose a technique verified by Jia et al. (2021) inspired by the acceleration of flow obstructed by an LEV (see initial work: Wong et al., 2013):

$$U(d,t)|_{\text{z}} = \vec{u}_{\text{eff}}(z) \cdot \sin(\alpha_{\text{eff}}) \left(2 + \frac{R^2_{\text{LEV}}(z,t)}{r^2_{\text{LEV}}}\right) \ , \tag{1.4}$$

where d is the shear-layer thickness, R_{LEV} is the radius of the vortex area, and r_{LEV} represents the distance from the vortex center. The vortex area radius is easily defined with a relationship between the vortex area, the mass entering the leading-edge shear-layer and the fluid density.

1.1.4 Circulation Transport Through Spanwise Flow

The spanwise flow within an LEV is known to be a critical parameter for the mass-particle transport along the span. Modelling the spanwise flow offers an investigation of the role of circulation transport and its effect on the circulation growth. Nonetheless, its distribution is complex to model for a rotating wing as it must consider the rotational acceleration and the pressure gradient components along the span, which are coupled together. For example, Van Den Berg and Ellington (1997) suggested that the spanwise flow is governed by the dynamic pressure gradient, generated by the velocity fields along the span, which is resulting from the centrifugal acceleration due to the rotation of the wing. Following this idea, Maxworthy

(2007) modelled the pressure gradient generated from the centrifugal effects for a quasi-steady LEV on a rotating wing and the resulting distribution of circulation. The model suggested by Maxworthy (2007) couldn't be adapted to our case, since it requires the vortex area along the span, which is one of the unknowns we seek to predict. Thus, the present work aims to estimate the spanwise flow distribution magnitude for a rotating wing with Bernoulli's equation in a rotating coordinate system, such that it is characterized by both the rotational acceleration and the pressure gradient. The general equation is modified to represent the flow conditions. After a simplification by assuming spanwise flow is zero at the axis of rotation, and by assuming a linear pressure gradient in the case of a purely rotating wing (see: Limacher et al., 2016), the modified equation after reorganisation is presented as:

$$w^2 = \frac{2k}{\rho}\frac{\partial P}{\partial z}z + \Omega^2 z^2 \ . \tag{1.5}$$

where P is the local pressure, Ω represents the rotational speed and z is the distance from the axis of rotation (and Z_T is then equivalent to the wing tip position within that domain). The assumption that the spanwise flow expression can be derived from Bernoulli equation, would be validated if the curve-fit obtained from experimental spanwise flow measurements into a second-order polynomial is similar to the curve obtained by plotting w versus z from Equation 1.5. The relative influence of both the pressure gradient and of rotational accelerations will then be determined from the curve-fit coefficients magnitude.

1.2 Contributions of the Current Work

The body chapters of this thesis consist of two research articles submitted for publication. Together, they test each of the four above hypotheses. The first article, presented in Chapter 2, focuses on the modelling exercise itself. The model is adapted such that it doesn't rely on experimental data input. The model investigates the role and the magnitude of both the circulation generation and its transport and offers accurate modelling solution to characterize them. The second article, presented in Chapter 3, focuses on the physics and dynamics of

the model concept. The core assumptions, fundamental to the model concept, are tested. The purpose is to understand the flow behaviours characterized by the vorticity transport equation and their role within an LEV on a thin flat plate in rotation, such that it can be interpreted as species transport.

Both articles compare the circulation distribution predicted by the model against experimental circulation values obtained with PIV to validate the model and the intermediate results. As the model presented in Chapter 3 is strictly used as a tool to test the underlying flow physics, rather than the model itself, the model is only semi-empirical, such that both the shear-layer velocity and the spanwise flow profile are parameters controlled by experimental values, whereas they are modelled in Chapter 2. Although the shear-layer velocity is extracted directly from experimental velocity fields in Chapter 3, the experimental spanwise flow is translated into a curvefit inspired from a modified Bernoulli equation.

Modelling the shear-layer velocity profile and the spanwise flow distribution in Chapter 2 tackles two of the initial goals. The study offers model solutions to characterize the circulation generation through the leading-edge shear-layer and the circulation transport through the spanwise flow. On the other hand, replacing the shear-layer velocity profile and the spanwise flow distribution by empirical inputs isolates the underlying physical assumptions for validation, such that an investigation of the circulation transport properties can be achieved. If the species transport model concept is applicable, the present work will have achieved its main goal of offering a circulation model for an LEV on a rotating wing.

Chapter 2

A Species-transport Model for Circulation in a Leading-edge Vortex

In this study, we propose a model to predict circulation growth along the span of a rotating wing, in which circulation transport is represented as species transport. Fluid particles entering the vortex shear-layer at the leading edge are initialized as vorticity-containing mass and are advected by the flow along the span. A circulation budget is presented, consisting of a generation and transport term, the latter derived from the vorticity transport equation, which leaves only two unknowns for the modeller to determine: the shear-layer thickness and the spanwise flow distribution. We find that the model is insensitive to the value chosen for the shear-layer thickness, as varying the thickness by an order of magnitude only changes the output by a few percent. Meanwhile, we use Bernouilli equation in a rotating coordinates system as a basic model for spanwise flow. To verify the accuracy of the model, the predicted circulation values are compared against experimental circulation values and show good agreement to measurements close to the axis of rotation, which corresponds to the spanwise locations at which the spanwise flow model best matches experimental data. It is suggested, therefore, that this model produces accurate results subject to an appropriate spanwise flow model.

2.1 Introduction

Leading-edges vortices (LEVs) often present highly three-dimensional flow characteristics, which makes modeling difficult. However, understanding their dynamics is essential for understanding biological locomotion, or using such locomotion to develop engineered flyers (see: Rival et al., 2010; Rival and Tropea, 2010; Rival et al., 2014). The present work will provide a circulation growth model for a rotating wing that accounts for some of these three dimensional characteristics. The model will estimate the circulation distribution from the flux of circulation through the leading-edge shear layer and its transport through the spanwise flow.

2.1.1 The Circulation Balance of an LEV

Modelling the circulation growth of an LEV in three-dimensional flows, such as flapping or rotating wings, is challenging because the circulation at any given spanwise location and the spanwise transport of circulation at that location tend to be coupled. For instance, many previous modelling efforts have required knowledge of the vorticity field to determine spanwise flow (for example, see: Maxworthy, 2007). One possible simplification is to model circulation transport as species transport, neglecting the complex vortex tilting behaviour, when the case permits (e.g., Wong and Rival, 2015; Wong et al., 2018). In this paradigm, the circulation transport is characterized by two terms: the circulation feeding rate $(\partial\Gamma/\partial t)_{\text{in}}$ and its spanwise transport via spanwise flow $(\partial\Gamma/\partial t)_{\text{out}}$. The circulation balance is thus expressed as:

$$\left(\frac{\partial\Gamma}{\partial t}\right)_{\text{total}} = \left(\frac{\partial\Gamma}{\partial t}\right)_{\text{in}} - \left(\frac{\partial\Gamma}{\partial t}\right)_{\text{out}}, \tag{2.1}$$

where Γ represents the circulation. For a stable LEV in steady state, such as that found on rotating wings, this balance must be zero. This simplication has been previously validated for a translating delta-wing, where spanwise flow is relatively constant (see: Wong et al., 2018).

The circulation feeding rate into the LEV is characterized by the vorticity generation within the shear layer. As shown by Didden (1979), a relationship can be established between the rate of circulation growth and the shear-layer velocity for a vortex generated by a piston-cylinder:

$$\left(\frac{\partial \Gamma}{\partial t}\right)_{\text{in}} = \frac{1}{2} u_o^2 \ , \tag{2.2}$$

where u_0 is the shear-layer velocity. A numerically identical result can be obtained for an LEV formed on a wing through a distinct derivation, in which mass enters and feeds the leading-edge vortex through the shear layer at the wing's leading edge, and likewise for the circulation generated in a boundary layer (see: Didden, 1979; Morton, 1984; Wong et al., 2018).

Since the circulation flux through the leading-edge shear layer depends strongly on the shear-layer velocity, the distribution of shear-layer velocity along the span must be determined. The shear-layer velocity distribution has been investigated in many studies, as its evaluation is tied to the understanding of the vortex growth. However, most of the available models or relationships to define the shear-layer velocity profile are confronted with unknown parameter limitations, such that their insights are difficult to adapt into a completely predictive tool. For example, Roshko (1954) provided a shear-layer velocity relationship with the free-stream velocity and the base-pressure coefficient:

$$u_o = U_\infty \sqrt{1 - C_{ps}} \ , \tag{2.3}$$

which is difficult to adapt as it would require the knowledge of the spanwise pressure profile. Indeed, knowing the pressure distribution along a wing's surface would likely eliminate the need for a vortex growth model, as the ultimate goal of such models is often to predict lift.

Other studies have attempted to model the shear-layer velocity by the acceleration of the flow around the blockage effect of the LEV (see: Wong et al., 2013; Jia et al., 2021):

$$u_o = U_\infty \cdot \sin(\alpha_{\text{eff}}) \left(1 + \frac{R_{\text{LEV}}^2(z,t)}{(R_{\text{LEV}} + d)^2}\right) + \frac{\Gamma(z,t)}{2\pi r_{\text{LEV}}} + \vec{u}_{\text{eff}}(z) \cdot \sin(\alpha_{\text{eff}}) \ , \tag{2.4}$$

where d is the shear-layer thickness, R_{LEV} is the radius of the vortex area, and r_{LEV} represents the distance from the vortex center, as depicted in Figure 1. This model has been independently applied to both rotating and flexible wings (Wong et al., 2013; Jia et al., 2021). The effective velocity $\vec{u}_{\text{eff}}$ is the local flow velocity, which is evaluated as $\vec{u}_{\text{eff}} = \Omega \cdot z$ for the specific case of a wing in pure rotation, as will be investigated in this study.

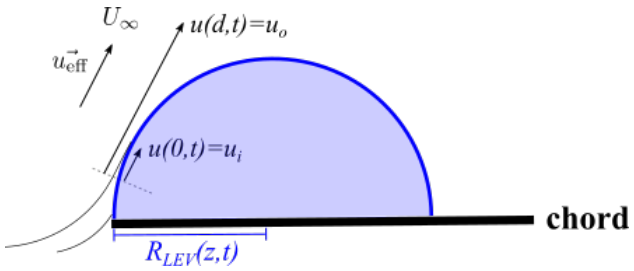

Figure 2.1: Integration approximated area for the velocity field around the boundary of the shear-layer of an LEV, represented as a semi-cylinder of radius $R_{\text{LEV}}(t,z)$.

This model requires modelling the vortex area itself, in addition to the circulation of the vortex. As circulation enters the LEV with mass through the leading-edge shear layer, the relationship between area (or radius) and mass is straightforward via density:

$$R_{\text{LEV}}(t) = \sqrt{\frac{2}{\pi\rho} m'(t)} \ , \tag{2.5}$$

where the mass per unit span m' is evaluated by integrating the mass entering the vortex through the leading-edge shear layer, minus the mass removed through spanwise flow as:

$$m(t)|_{\text{z}} = \rho \int \left(d\frac{u_i + u_o}{2} \Delta z - \iint_A w(z,r,t) \cdot \vec{n} \mathrm{d}A \right) \mathrm{d}t \ , \tag{2.6}$$

where z is a spanwise position and Δz is a spanwise element such as in a strip-theory calculation. This expression for the mass flux into the LEV includes an extra term to account for the mass transport due to spanwise flow. Here, $w(z,r,t)$ represents the spanwise component of velocity and A represents the area of the LEV.

As the spanwise flow removes mass along the spanwise direction, it also removes circulation. The circulation transport can be determined by integrating the vorticity-transport equation over the vortex area. Taking an average across the vortex area, this value has been determined to be (see: Wong and Rival, 2015):

$$\frac{\partial \Gamma}{\partial t} = \overline{w}\frac{\partial \Gamma}{\partial z} \ , \tag{2.7}$$

where the overbar here represents a spatial average. There are many ways to approach implementing the above equations as a predictive model. However, it is worth noting that by neglecting vortex tilting, we have already made the assumption that circulation follows the mass in the flow. This is a reasonable assumption far from the tip vorticies (see: Cheng et al., 2013). Therefore, we propose a particle-based model that tracks mass and circulation simultaneously. This combines previous work that either tracked only circulation (Wong et al., 2018), or tracked circulation and mass as distinct properties without such a particle-based approach, and includes implicitly the assumption above of low vortex tilting (Wong et al., 2013; Jia et al., 2021).

2.1.2 Species Transport Model

Recent attempts to model the spanwise transport of circulation by species transport have proven helpful in accounting for the large number of unknowns in such a modelling process. However, these models attempted to track circulation alone. As the area of the LEV could not be computed with only circulation known, this limited the means by which the shear-layer velocity could be estimated. Here, we propose to adapt the shear-layer velocity model presented in Section 2.1.1 to such particle-based models by tracking mass simultaneously.

The basic outline of the model is shown in Figure 2.2. At each time step, particles representing mass are initialized uniformly across the wing span. Each particle is assigned a mass and circulation based on the shear-layer properties at that time step, and are then allowed to advect along the span, as shown in Figure 2.3. At any given timestep, the total mass or circulation at a spanwise location is the sum of all the particles at that location —

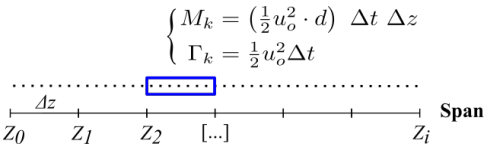

Figure 2.2: At every time-step t, N fluid particles representing vorticity-containing mass are initialized uniformly along the spanwise domain Z discretized in i bins. Each particle represented by the subscript k is initialized by the local mass M_k and circulation Γ_k divided equally among all the particles contained in the same bin.

both those generated that time step, and those advected into that location over time.

Modelling the mass of the vortex with this particle-based method requires modifying the equations shown in Section 2.2. For instance, the mass flux into a spanwise section, shown in Equation 2.6, no longer has to consider spanwise flow explicitly, as the motion of the particles will account for that. Therefore, particles are instead initialized by the value:

$$m(t)|_{\mathrm{z}} = \rho \left(d \frac{u_i + u_o}{2} \Delta z \right) \mathrm{d}t \ . \tag{2.8}$$

Meanwhile, the shear-layer velocity estimate in Equation 2.4 was derived using a different method for determining circulation. Removing that term gives the shear-layer velocity as:

$$U(d,t)|_{\mathrm{z}} = \vec{u}_{\mathrm{eff}}(z) \cdot \sin(\alpha_{\mathrm{eff}}) \left(2 + \frac{R^2_{\mathrm{LEV}}(z,t)}{r^2_{\mathrm{LEV}}} \right) \ . \tag{2.9}$$

As such, the only variable that the modeller must assign a value *a priori* is the shear-layer thickness d in order to assign an initial value to any given particle. One therefore only requires a model for spanwise flow in order to model the entire LEV growth.

2.1.3 Spanwise Flow Circulation Transport Models

The circulation transport described in the previous section is sensitive to the spanwise flow. The spanwise flow component in the present work plays an important role as it defines mass-particle transport along the span. Previous studies have described the spanwise flow distribution in an LEV on a rotating wing considering both the centrifugal acceleration distribution and the pressure gradient along the span. Moreover, these terms appear to be coupled. For instance, Van Den Berg and Ellington (1997) suggested that the spanwise

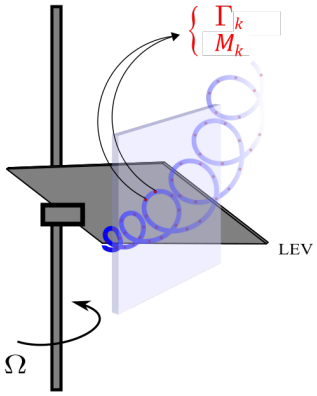

Figure 2.3: Fluid particles representing vorticity-containing mass enter the shear layer of the LEV and is advected through the flow along the span. Following the species transport model concept, each particle is initialized with mass and circulation information.

flow is governed by the dynamic pressure gradient resulting from the velocity distribution along the span, itself generated by the centrifugal acceleration resultant from the rotation of the wing. Following this idea, Maxworthy (2007) characterized the pressure gradient along the span for a quasi-steady LEV on a rotating wing. The model from Maxworthy (2007) determined the pressure gradient that resulted from both the centrifugal effects as well as the distribution of circulation. Unfortunately, the model may be better suited to retroactively investigate a flow than as a predictive model, since it requires the vortex area, which is one of the terms we seek to compute. While this model provides key insight into the flow within the LEV, it cannot be easily adapted to the present case.

Therefore, to estimate the magnitude of the spanwise flow distribution for a rotating wing, we will implement a simpler model. The spanwise flow distribution given by Bernoulli's equation in rotating coordinates for an inviscid flow is:

$$\frac{P}{\rho g} + \frac{w^2}{2g} - \frac{z^2\Omega^2}{2g} = \text{const} \ , \tag{2.10}$$

where P represents the local pressure, g represents the gravitational acceleration and z represents the distance from the axis of rotation, such that Z_T would represent the wing tip position within that spanwise domain. Assuming spanwise flow is zero at the axis of rotation, and assuming a linear pressure gradient (see: Limacher et al., 2016), the equation

becomes:

$$w^2 = \frac{2k}{\rho}\frac{\partial P}{\partial z}z + \Omega^2 z^2 \ , \tag{2.11}$$

where Ω represents the physical rotational speed. It will be shown later that, at least for our case, the entire pressure gradient term is small, in which case the resulting spanwise flow can be reasonably modelled as:

$$w^2 = \Omega^2 z^2 \ . \tag{2.12}$$

While this model is imperfect, of course, it is worth noting that previous results concerning LEV stability can be recovered despite its simplicity. For instance, if we take the spanwise transport of circulation, and normalize Γ by $U_\infty c = \Omega Z_T c$, normalize the gradient in z by Z_T, and the spanwise flow by ΩZ_T, then the normalization follows as:

$$\left(\frac{\overline{w}}{\Omega\ Z_T}\right)\left(\frac{\partial\Gamma}{\partial z}\ \frac{Z_T}{(\Omega\ Z_T)\ c}\right) = \overline{w}\ \frac{\partial\Gamma}{\partial z}\ \frac{1}{(\Omega\ Z_T)^2}\ AR = \Pi_0 \ . \tag{2.13}$$

where it is presumed that this spanwise transport of circulation forms a Pi group, $\Pi_0 = f(\Pi_1, ...)$. Therefore, the dimensional transport of circulation should scale with $1/AR$, such that lower aspect ratios correspond to more stable LEVs, which corresponds to the findings of Lentink and Dickinson (2009a,b).

2.2 Methodology

To validate the circulation growth model, we will test the predicted values against experimental results under matching flow conditions. Particle Image Velocimetry (PIV) is used to evaluate the flow field at several spanwise positions, as well as in the spanwise direction. In addition to validating the total circulation values, the PIV measurements can be used to evaluate the shear-layer velocity and spanwise flow estimates produced by the model.

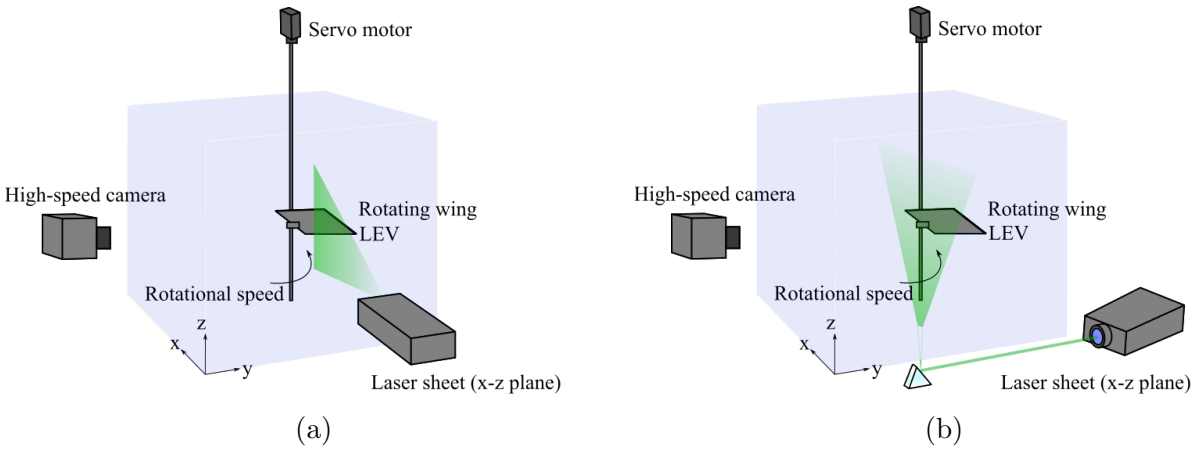

Figure 2.4: Experimental set-up for (A) the spanwise flow measurements (B) the LEV circulation growth measurements. In both cases, the laser sheet plane is parallel to the camera.

2.2.1 Parameter Space Selection

The circulation growth model assumes limited vortex tilting, and therefore the parameter space has been selected in order to minimize the effect of tip vorticies. A continuously rotating wing also generates a stable LEV, which, while not strictly required, does simplify the measurement process. Therefore, we will evaluate the model in the case of a thin flat plate in rotation, at an angle of attack of 45 degrees. Reynolds numbers are selected to be low ($Re = 1000$ and $Re = 2500$), in order to maximize the effect of viscosity in order to test the assumption that viscous effects were small. The Reynold number is then defined as:

$$Re = \frac{\rho \, \Omega \, Z_T \, c}{\mu} \ , \tag{2.14}$$

such that the Reynolds numbers are evaluated at the wing tip, where ρ represents the density and μ represents the water viscosity. The selected positions are defined as the distance from the axis of rotation but will be referred to as their position from the root of the wing. Their values include the $0.5c$ gap distance from the axis of rotation to the root of the wing. The wing has a chord of $c = 50.8$ mm (2 in), a span of $b = 210$ mm and a thickness of $\tau = 3.2$ mm (1/8 in), giving an overall aspect ratio of 4. The wing was rotated within a cubic tank of 1 m^3. The dimensions satisfy the wing clearance criteria described by Manar et al. (2014).

The spanwise locations are all in the inner-half of the span, in order to minimize the

effect of the tip vortex and, therefore, minimize the effect of vortex tilting. Measurements were therefore taken at 1/4, 1/3, and 1/2 of the span length, from the root to the wing tip. The wing was rotated at a constant rate by a stepper motor. To achieve the low rotational speeds required by the selected Reynolds numbers, a 27:1 planetary gear reduction was placed between the stepper motor (Longrunner 22B, 200 step-per-revolution) and the drive shaft.

2.2.2 Optical Set-up

Two optical set-ups were used to capture the flow within the vortex core and the spanwise flow, respectively, as shown in Figure 2.4. The PIV setup consists of a Photron FASTCAM Mini WX-50 high-speed camera with a Tamron 100 mm/2.8 lens. A 6.5 W continuous wave-laser was used to illuminate the flow field, seeded with polymer microbeads as seeding particles. The image resolution was $2048 \times 2048\,\text{pixel}^2$ with a pixel size of 10μm. The specific frame rate varied between individual test cases as a function of the local flow velocity. Vector fields computed in LaVision Davis 10.

Measurements were repeated at several azimuthal angles, in order to observe any time-dependence in the LEV strength or shear-layer velocity. The selected revolution angles range varies from 90 degrees to 225 degrees with increments of 45 degrees, such that effects from the impulsive start are excluded. Therefore, from here on, azimuthal angle and time may be used interchangeably.

A median normalization was applied prior to vector calculation to subtract the background image for each run. Ten runs were recorded for each case. After the median normalization, only frames where the LEV presents perpendicular to the camera were kept to be processed. Flow fields were calculated with a multi-grid/multi-pass cross-correlation algorithm. For each study case, an overlap of 50% was applied to the first two passes with the initial interrogation window and an overlap of 75% was applied to the last two passes. Asymmetric interrogation windows were utilized for spanwise flow calculations.

2.3 Results and Discussion

Outputs from the model are presented in Figure 2.5 for the $Re = 2500$ case. The $Re = 1000$ case is similar. As the model is tracking particles representing circulation-containing mass, the mass distribution within the LEV is presented as well in Figure 2.5. As shown in Figure 2.5, the distribution of mass into the LEV is approximately linear with the span while the circulation growth grows slightly faster along the span.

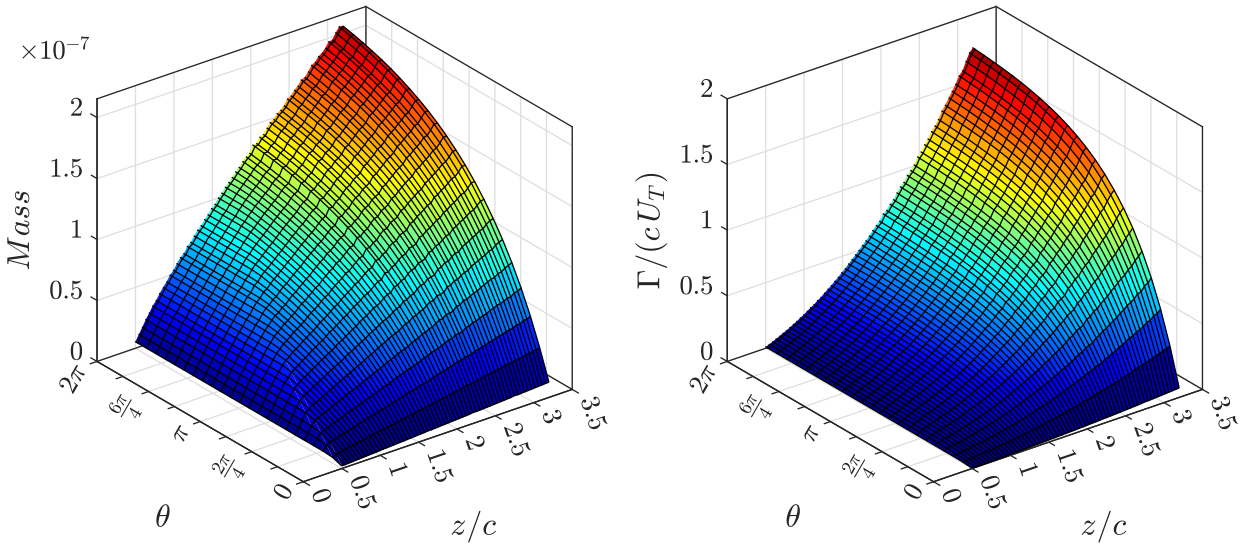

(a) (b)

Figure 2.5: (A) The mass growth within the LEV along the span of a rotating wing is an approximately linear distribution while (B) the circulation growth along the span of a rotating wing is growing faster. Both the mass m and the circulation Γ^* distributions are presented in function of the span position z^* and in function of the time, or the equivalent revolution angle $t^* = \theta$. The figure presents the $Re = 2500$ case, but the behaviours for the $Re = 1000$ are similar.

The circulation estimated by the model is compared to experimentally measured circulation values in Figure 2.6. The experimental circulation values are presented as broken lines while the modelled circulation values are presented as a shaded range with matching colors to indicate each spanwise position. The shaded region for the modelled values represent the range of circulation estimates obtained by varying the shear-layer thickness d by one order

of magnitude, from $d = 10^{-3}$ m to $d = 10^{-2}$ m. As the shear-layer thickness is the only parameter the modeller can vary, this demonstrates that it has a negligible outcome on the output of the model. This is desirable, as the model is still useful without any *a priori* knowledge of the flow field, and the modeller only requires a rough guess of the shear-layer properties. Matching colors indicate identical spanwise position for easier visualisation. As shown in Figure 2.6, the model is robust and minimally sensitive to the shear-layer thickness parameter input.

The modelled shear-layer velocity controls the circulation feeding term, while the modelled spanwise flow distribution controls the circulation transport. Eventually these terms find equilibrium, and the vortex is considered stable. However, the modelled circulation is in best agreement closer to the axis of rotation (1/4 and 1/3 of the span). This coincides to the regions along the span with the greatest agreement between modelled and measured spanwise flow, indicating that the quality of the spanwise flow model is the primary limiting factor in a circulation model of this type, which is discussed in the following section.

2.3.1 Spanwise Flow Approximation by Bernoulli's Equation

The experimental spanwise flow is shown in Figure 2.7, alongside the modelled values. Fitting modified Bernoulli equation to the experimental data, the pressure gradient term contributes very little to the overall spanwise flow, using the rotational term contributing more than 95% of the total magnitude. While Bernoulli equation in rotating coordinates estimates the magnitude the spanwise flow with both rotational and pressure terms, fitting the equation terms to the experimental data shows that the spanwise flow is driven mostly by the rotational acceleration, and the pressure variation $\partial P/\partial z$ represents less than 5% of the total spanwise flow.

The modelled values therefore include only the rotational components, based on the physical rotation rate of the wing. As seen in Figure 2.7, the modelled spanwise flow values are initially a good fit with the experimental data, but deviate from the experimental data with increased span. This the likely reason that the predicted circulation values in Figure

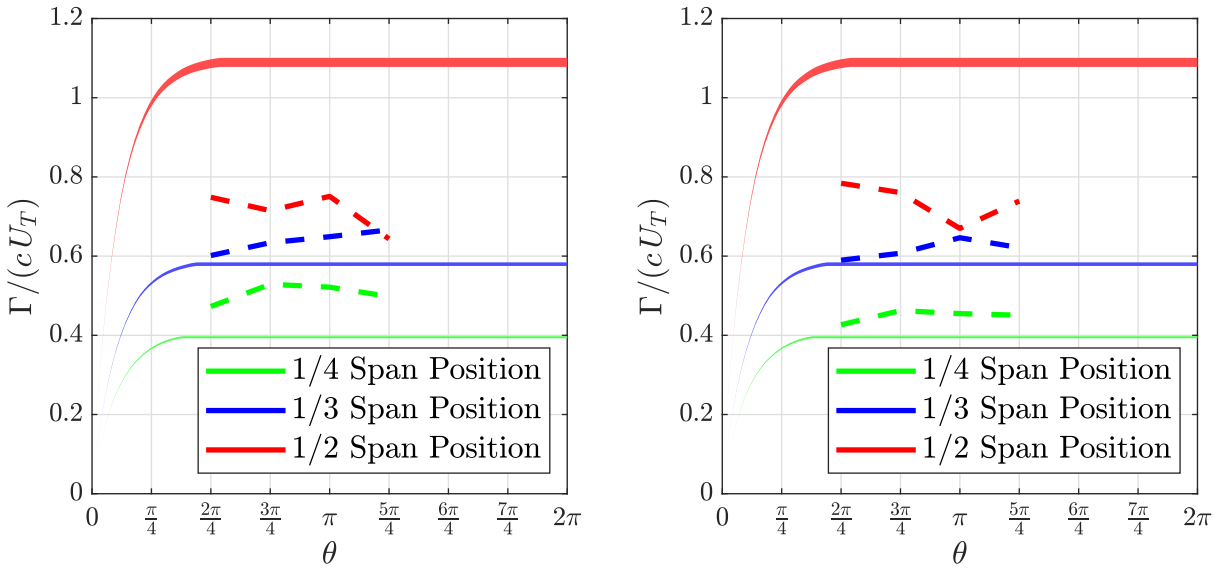

(a) (b)

Figure 2.6: Circulation versus time for each spanwise position for (A) $Re = 1000$ and (B) $Re = 2500$. The modelled circulation predictions (shaded areas) are overall similar to the experimental circulation values (broken lines). Matching colors identify each spanwise location. The shaded area represents the prediction interval relative to the shear-layer thickness d parameter sensitivity. The behaviours for both Reynolds numbers are similar as the model was found to be insensitive to Reynolds numbers.

2.5 are in good agreement closer to the axis of rotation, but are overestimated farther along the span. As the circulation transport depends directly on spanwise flow, this results in the over-estimate of circulation by the model previously observed in Figure 2.6. However, it also shows that the model performs adequately as long as spanwise flow estimates are accurate.

2.3.2 Shear-Layer Velocity Profile Approximation

To model the circulation generation, the distribution of the shear-layer velocity must be estimated. As mentioned previously, the outer shear-layer velocity is the primary value characterizing the shear layer at the leading-edge, as the inner shear-layer velocity is small. Experimental velocity values are obtained by sampling the velocity at the location of maximum shear. Values were sampled at several locations along a line normal to the velocity vector at this location of maximum shear, and the maximum velocity along this line is taken

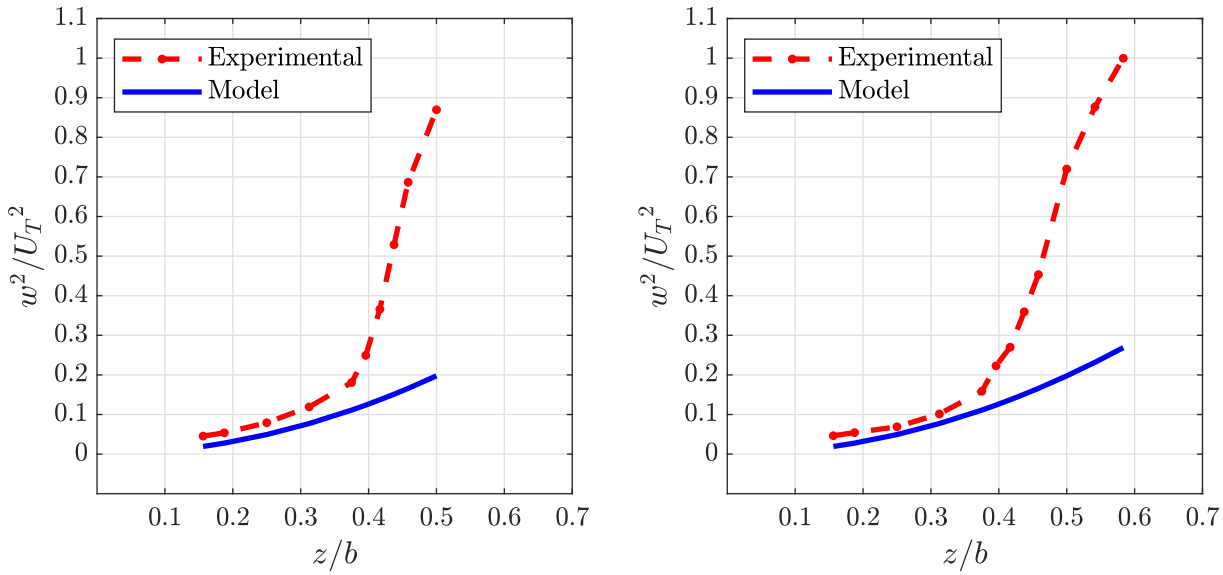

(a) (b)

Figure 2.7: Curve fits of the spanwise flow when constrained to match the form suggested from Bernoulli equation in rotating coordinates for (A) $Re = 1000$, and (B) $Re = 2500$. Experimental spanwise flow is presented with a broken line while the spanwise flow model is presented with a solid line. Spanwise flow is presented from 1/4 to 1/2 of the span. In both cases, spanwise flow is primarily driven by rotational acceleration rather than the pressure gradient.

as the outer shear-layer velocity.

The modelled shear-layer velocity is compared to the experimental shear-layer velocity in Figure 2.8 for both $Re = 1000$ and $Re = 2500$. There is little difference between the Reynolds number cases, which was expected due to the insensitivity to Reynolds number on LEV topology seen in the literature (see: Baik et al., 2012; Garmann et al., 2013). The experimental shear-layer velocity, shown as the blue dashed line, grows along the span. The modelled shear-layer velocity presented in solid line is also a nearly-linear distribution along the span within the experimental range. While the modelled shear-layer velocity is somewhat under-estimated at the root of the wing, the values converge as we reach the half-span location. In general, the model is less sensitive to accurate shear-layer velocities and thicknesses than to spanwise flow values, and therefore we believe the values given here are acceptable for the purposes of the model

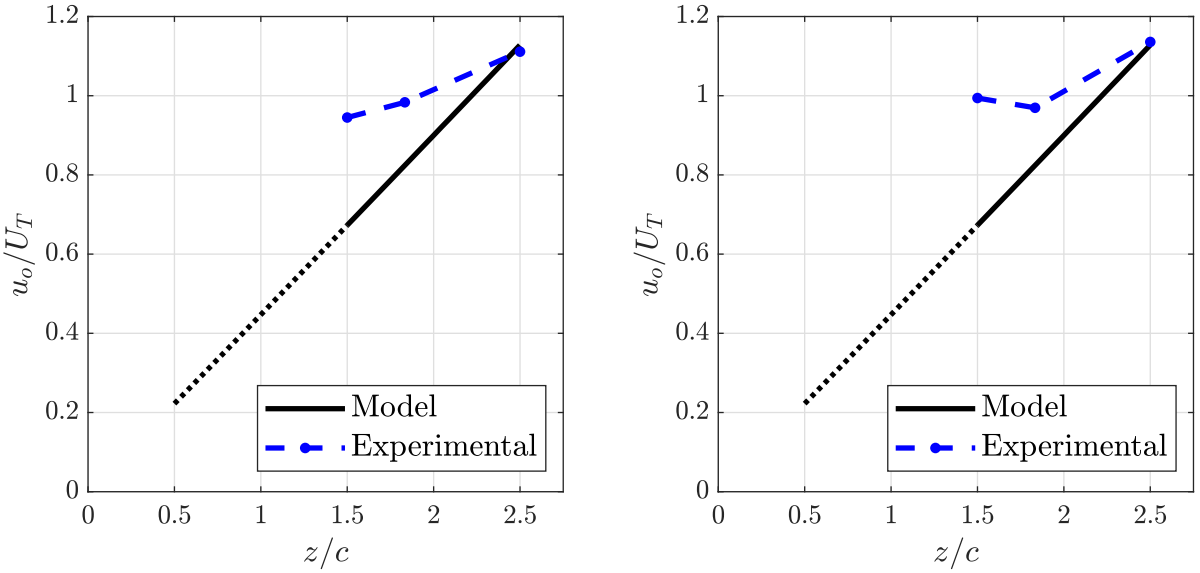

Figure 2.8: Predicted shear-layer velocity profile along the span versus experimental shear-layer velocity distribution (from 1/4 to 1/2 of the span) for (A) $Re = 1000$ and (B) $Re = 2500$. The predicted values are identified by a solid line only for the spanwise region of interest and becomes a dot line to represent the projected values of the spanwise region between the root and 1/4 of the span. When normalized by the wing tip velocity, the shear-layer velocity profile for both Reynolds numbers are similar, if not identical.

2.4 Conclusion

The purpose of this exercise was to provide a predictive model for the LEV circulation distribution along the span of a rotating wing. The model for spanwise circulation transport is derived from the approximation of the vorticity transport equation as species transport, such that circulation is tied to the mass entering the LEV's shear-layer. The model originally only accounted for circulation transport, and not mass transport, requiring the use of empirical values for the shear-layer velocity. The addition of mass transport to the model here permitted the use of a shear-layer velocity model, reducing the dependence on empirical data.

Given an appropriate and accurate spanwise flow model, the transport model accurately predicted the circulation of an LEV. However, in regions where the spanwise flow model

underestimated spanwise velocity, circulation values were over-estimated as the spanwise transport of circulation was under-estimated. This shows the need for a better model for the spanwise flow in a leading-edge vortex. Nevertheless, the model proved to be a simple and effective methodology to estimate the LEV circulation growth along the span for a rotating wing, in situations where vortex tilting is not expected to be significant.

Chapter 3

The Vorticity Budget of the Leading-edge of a Rotating Wing

In order for a leading-edge vortex (LEV) to reach steady-state, the flux of circulation into the vortex from the leading-edge shear-layer must be balanced. Vorticity annihilation mediates LEV circulation by entraining mass of opposite-signed circulation from near the wing surface. However, this circulation cannot originate through the wing surface, as there is no flow normal to the surface, so where does it come from? To answer this question, we model circulation transport within an LEV as simple species transport - circulation is carried by mass through the flow - and compare it to a reference case. The difference between these two cases may provide insight into the role of annihilation. To maximize similitude between the model and reference, we use a semi-empirical approach, matching measured shear-layer feeding velocity and spanwise flow. However, we find no appreciable difference between modelled and measured circulation, suggesting that the opposite-signed circulation may already accounted for by the flux of circulation through the leading- and trailing-edge shear-layers, depending on control volume selection.

3.1 Introduction

Leading-edge vortices (LEVs) are ubiquitous in both biological and engineered swimmers and flyers at small scales. Therefore, proper understanding of LEV dynamics equip us to better understand both ecology and small aircraft design, such as UAVs. However, current descriptions of LEV growth and development are limited by our understanding of vorticity transport. The role of the circulation convection when in presence of spanwise flow — such as in the case of a rotating wing — and the magnitude of circulation generation in the leading-edge shear layer must be modelled with care. In particular, it is not yet clear if these two terms are the only relevant terms in determining the circulation budget of a rotating wing.

3.1.1 Modelling Circulation Growth in Leading-edge Vortices

Models for circulation growth of LEVs, such as those by Hemati et al. (2014) or Ramesh et al. (2014), can be used to both better understand the LEV formation process itself, and to generate models for force generation. Many models for circulation growth can be broken down into two primary types: *point vortex models*, in which point vorticies of constant strength are shed in accordance with the so-called leading-edge suction parameter (LESP), and *shear-layer feeding models*. A brief description of each is provided below.

The Leading-Edge Suction Parameter and Point Vortex Models

Polhamus (1966), developed a leading-edge suction analogy from thin airfoil theory to model and investigate the LEV found on delta wings. The LESP re-emerged in the 2010s as a technique to describe LEV formation on low-Reynolds number flyers. For example, Ramesh et al. (2014, 2018) studied the initiation of the LEV, and showed the criticality of the LESP, which is derived from boundary layer theory and applied to potential flow theory, in predicting vortex formation. His work showed that the seperation of the boundary layer at the leading edge could be parameterized via the LESP. The LESP was used as a criterion in a potential flow model to determine if and when a point vortex would be initiated in the

flow (i.e. point vorticies are generated until the LESP suggests separation no longer occurs). In addition to its utility as a predictive tool, the study showed that the LESP could be used retroactively to characterize the kinematics and the aerodynamic parameters that lead to LEV formation. In the more recent years, Deparday and Mulleners (2019); Deparday et al. (2022) and Narsipur et al. (2020) have been investigating the use of the LESP as a fully unsteady parameter, rather than quasi-steady. Whereas the LESP can determine when separation will occur, shear-layer models investigate the dynamics in a separated shear layer itself.

Shear-layer Feeding

As early as 1979, Didden described a relationship between velocity scale and vortex roll-up in vortex rings generated in piston-cylinder experiments (see: Didden, 1979). It is possible to translate this work to the similar process of vortex roll-up from any other shear layer, such as the LEV on a wing. For example, Wong et al. (2018) developed a predictive vortex growth model applied to a steady translating delta wing. The model gave the rate of circulation growth, taking the same form predicted by Didden, as:

$$\frac{\partial \Gamma}{\partial t} \propto u_o^2 \,, \tag{3.1}$$

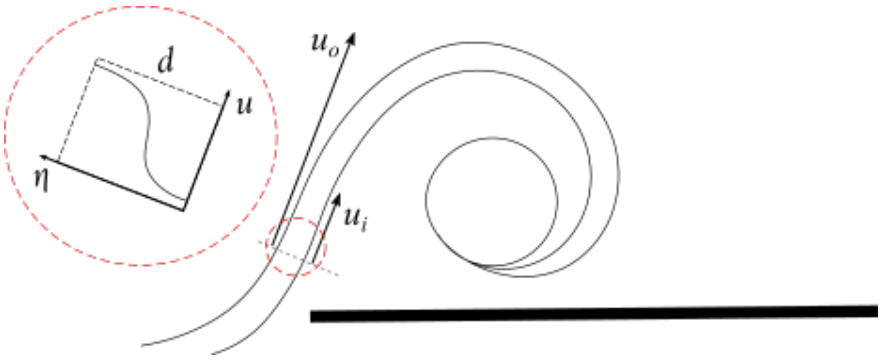

Figure 3.1: Integration area for the velocity field around the boundary of the shear layer of an LEV.

where Γ represents the strength of the LEV and u_o is the outer shear-layer velocity. Analyzing the velocity field presented in Figure 3.1, the circulation flux was determined by considering

the circulation flux as the product of the mass flux into the LEV, and the circulation per unit mass in the shear layer:

$$\left(\frac{\partial \Gamma}{\partial t}\right)_{\text{in}} = \frac{\partial \Gamma}{\partial m'} \frac{\partial m'}{\partial t} \ , \tag{3.2}$$

where m' is the mass in the leading-edge shear layer per unit span, $m' = \rho dl$, ρ is the density of the fluid, d is the shear-layer thickness and l is a characteristic shear-layer length. The circulation in the LEV is then evaluated by path integral as $\Gamma = u_o l$ where u_o is the outer shear-layer velocity (this assumes the inner shear-layer velocity is small). The terms in Equation (3.2) can therefore be evaluated as:

$$\left(\frac{\partial \Gamma}{\partial t}\right)_{\text{in}} = \left(\frac{u_o l}{\rho dl}\right)\left(\frac{1}{2}\left(u_o + u_i\right)\rho d\right) = \frac{1}{2}\left(u_o^2 + u_o u_i\right) \ , \tag{3.3}$$

where the mass flux is approximated by the trapezoidal rule. If the inner shear-layer velocity (u_i) is negligible compared to the outer shear-layer velocity, the resulting vorticity flux is $\partial\Gamma/\partial t = \frac{1}{2}\, u_0$.

However, by default both LESP and shear-layer based models only consider the two-dimensional problem of circulation entering an LEV. For highly three-dimensional flows, such as those on rotating wings, we must consider the spanwise transport of circulation.

3.1.2 Three-dimensional Vorticity Transport

Spanwise flow can transport circulation along the axis of a vortex as described by the vorticity transport equation. However, the extent to which circulation is tied to mass is controversial. In the present work we wish to investigate the extent to which circulation transport can be approximated as species transport, and to do so will require a discussion of the transport equation.

The Vorticity Transport Equation

The vorticity transport equation for an incompressible fluid is:

$$\frac{\partial \vec{\omega}}{\partial t} + (\vec{u} \cdot \nabla)\vec{\omega} = (\vec{\omega} \cdot \nabla)\vec{u} + \nu \nabla^2 \vec{\omega} \ . \tag{3.4}$$

The left hand side is the advection of vorticity, while the right hand side is vortex stretching and tilting and viscous diffusion of the vorticity. The present work will consider a nearly two-dimensional vortex, with limited influence from tip vorticies, such that the tilting terms can be ignored. However, as the focus is on the transport of circulation rather than vorticity, it must be noted that circulation is conserved under vortex stretching. Under similar conditions, Cheng et al. (2013) showed that vortex stretching and tilting had minimal effect on the circulation balance of a rotating wing, compared to convection.

As a stable vortex must have a constant circulation, some circulation must be removed from the vortex in order to balance circulation flux from the leading-edge shear layer. The rate at which circulation is removed from the vortex through spanwise convection can be calculated by integrating the vorticity-transport equation over the vortex area. This yields:

$$\frac{\partial \Gamma}{\partial t} = \overline{w} \frac{\partial \Gamma}{\partial z} \ . \tag{3.5}$$

By comparing this value to the circulation flux into the LEV from the leading-edge shear layer, a circulation balance is obtained:

$$\left(\frac{\partial \Gamma}{\partial t}\right)_{\text{total}} = \left(\frac{\partial \Gamma}{\partial t}\right)_{\text{in}} - \left(\frac{\partial \Gamma}{\partial t}\right)_{\text{out}} = \frac{1}{2} u_o^2 - \overline{w} \frac{\partial \Gamma}{\partial z} = 0 \ , \tag{3.6}$$

where $\overline{w}$ represents the average spanwise flow. This analysis has been previously presented in Wong et al. (2018). Moreover, it is repeated here as the present work wishes to investigate some of its core assumptions more carefully in the following sections. The above neglects the act of viscous diffusion, which are presumed to act over much larger timescales than of vortex growth. However, previous studies have shown that these terms may not be sufficient to describe the circulation balance (e.g., Wojcik and Buchholz (2014)).

Vorticity Annihilation

Recent studies, such as Wojcik and Buchholz (2014), Medina and Jones (2016), Onoue and Breuer (2017) and as summarized by Eldredge and Jones (2019), have investigated the effect of vorticity annihilation and its magnitude as a mechanism to balance the the circulation budget in an LEV. In these studies, vorticity annihilation was found to play an important role in the circulation budget. The circulation budget analysis presented by Wojcik and Buchholz (2014) was performed by inference, as a residual term within a transport or budget equation, while Onoue and Breuer (2017) measured the opposite-signed vorticity generated on the wing surface and entrained by the LEV. While this region of opposite-signed vorticity is readily identified in most measurements of LEVs, and it no doubt affects the local vorticity dynamics, it is unclear in which situations it and other terms must be included as a modelling exercise. Consider a control volume with one edge along the wing surface: as there is no velocity normal to the wing, there cannot be vorticity flux through the wing itself. If you wish to estimate the total circulation in the domain, then, would it be sufficient to account for circulation entering the volume elsewhere, i.e., through the shear layers? This study will attempt to answer exactly that question, by investigating just the shear-layer flux and spanwise convection in isolation.

The Role of the Spanwise Flow

The description of the circulation transport presented in the above sections depends strongly on the spanwise flow, which has proven difficult to model. As a solution to the axial flow distribution in a leading-edge vortex, Van Den Berg and Ellington (1997) suggested that the spanwise flow is governed by the dynamic pressure gradient generated by the velocity gradient along the wing, as the resultant centrifugal acceleration. Later, Maxworthy (2007) modeled a quasi-steady LEV for a rotating wing in order to characterize such a spanwise pressure gradient. He showed that the spanwise pressure distribution formed due to both centrifugal effects and the spanwise variation of circulation. As a secondary objective to investigating vorticity budget, this study will attempt to evaluate the relative magnitude of

each of these effects.

3.2 The Vortex Growth Model

The model, adapted from Wong et al. (2018), attempts to solve the limitations of unknown or difficult to estimate information for three-dimensional flows by treating the circulation transport as species transport. For the benefit of the reader, we will repeat a brief summary of the methodology here. The previous model does not provide guidance on how to predict spanwise flow or shear-layer velocity, and so we will discuss our treatment of these unknown terms here as well.

At every time-step, particles representing mass are initialized in a uniform distribution along the span of the wing. The circulation is locally evaluated as $\Delta\Gamma = \frac{1}{2}u_o^2\Delta t$, following Equation (3.3), and is divided equally among each of the N fluid particles. The particles are convected through the domain at the spanwise flow velocity. Therefore, at each time-step, the circulation at that point is the sum of the circulation of each of the particles at that spanwise location, including both particles generated that time-step, as well as those advected there from prior time-steps. The model was tested initially with the test case of a translating delta wing, such that the spanwise flow was assumed constant along the span, greatly simplifying the modelling exercise required to predict spanwise flow. In the case of a rotating wing, however, estimating the spanwise flow is a non-trivial task, and the present work therefore will utilize empirical data for this purpose. Likewise, empirical data is used for the shear-layer velocity as well. In this way, the model simulates a vortex subject exclusively to spanwise convection, as a means to investigate the role of vorticity annihilation. A characteristic output is shown in Figure 3.2 for input data discussed in later sections, generating a steady vortex with circulation growing from root to tip.

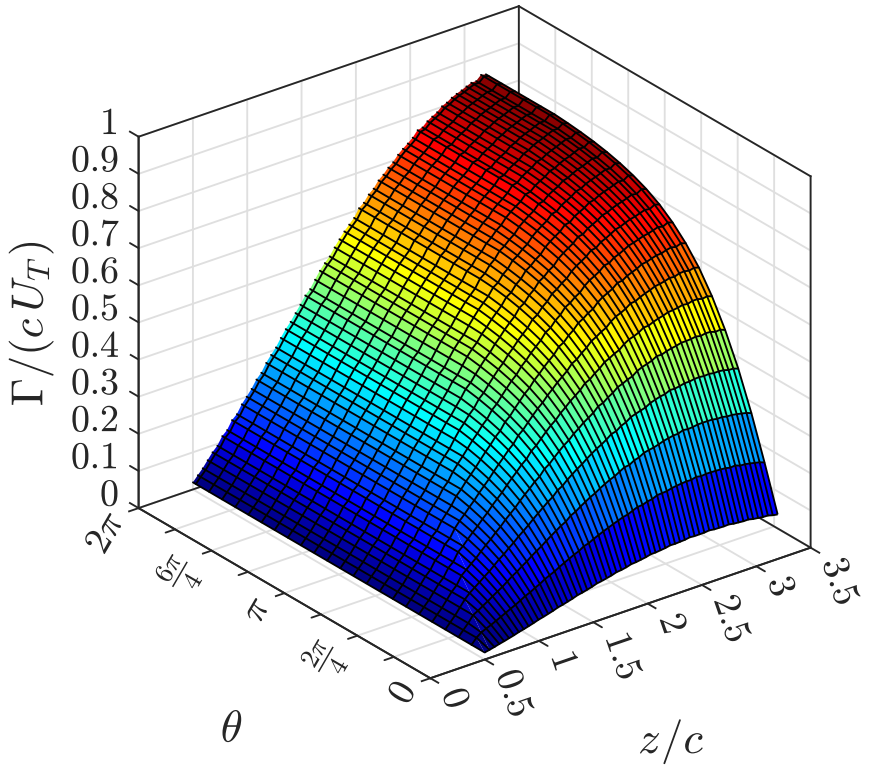

Figure 3.2: The circulation growth along the span of a rotating wing is approximately conical. The circulation variation is presented in function of the span position (from the root to 2/3 of the span) and the azimuthal angle. The figure presents the $Re = 2500$ case, but the behaviours for the $Re = 1000$ are similar.

3.3 Methodology

In order evaluate the large-scale circulation budget of an LEV, the flow field must be evaluated to both provide an input to the semi-empirical model, and a ground-truth with which to compare it. Separate planar PIV measurements are used to characterize the flow field at defined spanwise locations, and to determine the spanwise flow profile.

3.3.1 Parameter Space Selection

The current study investigates a thin flat plate under continuous rotation, at an angle of attack of 45 degrees. Low Reynolds numbers ($Re = 1000$ and $Re = 2500$) are used here to observe what effect, if at all, viscous effects have on the circulation budget. Considering ρ

as the density and μ as the water viscosity, the Reynold number is then defined as:

$$Re = \frac{\rho\,\Omega\,Z_T\,c}{\mu}\ , \tag{3.7}$$

where Ω is the rate of rotation (rad/s) and Z_T is the distance from the axis of rotation to the wing tip, which is slightly larger than the wing span b due to the $0.5c$ gap distance from the axis of rotation to the root of the wing. For clarity, the coordinate z, when used later on, is defined from the axis of rotation rather than the wing root. The spanwise locations selected for the PIV measurements are selected based on both the presence of a strong and constant LEV, but sufficiently far from the root and the tip of the wing to avoid significant vortex tilting terms associated with the tip vorticies affecting the measurements. Measurements were therefore taken at 1/4, 1/3, and 1/2 of the span. The velocity resulting from the rotation of the wing evaluated at the wing tip is presented as U_T.

The aspect ratio $AR = 4$ wing is fixed to a drive shaft centred in a $(1\,\mathrm{m})^3$ cubic tank and constrained to move in pure rotation. The wing has a chord of $c = 50.8\,\mathrm{mm}$, a span of $b = 210\,\mathrm{mm}$, and is a rectangular profile flat plate with a thickness of $\tau = 3.2\,\mathrm{mm}$. The dimensions satisfy the wing clearance dimensions suggested by Manar et al. (2014) to avoid tip vortex interactions with the enclosure walls.

A stepper motor is used to rotate the wing at a constant rotational speed. To achieve the low rotational speeds required by the above Reynolds numbers, the 1.8 degree-per-step (or 200 step-per-rotation) stepper motor was mated to a $27:1$ planetary gear reduction before the drive shaft.

3.3.2 Optical Set-up

Two optical set-ups were used to capture both spanwise flow and the vortex structure, respectively, as shown in Figure 3.3. The PIV setup consists of a Photron FASTCAM Mini WX-50 high-speed camera mated to a Tamron 100 mm/2.8 lens. A $6.5\,W$ continuous wave-laser was used to illuminate the flow field, seeded with polymer microbeads as seeding particles. The image resolution was $2048 \times 2048\,\mathrm{pixel}^2$ with a pixel size of $10\,\mu$mm. The specific frame rate

per second varied between individual test cases as a function of local rotational speeds and the particular Reynolds number of that test. Vector fields were calculated in LaVision Davis 10.

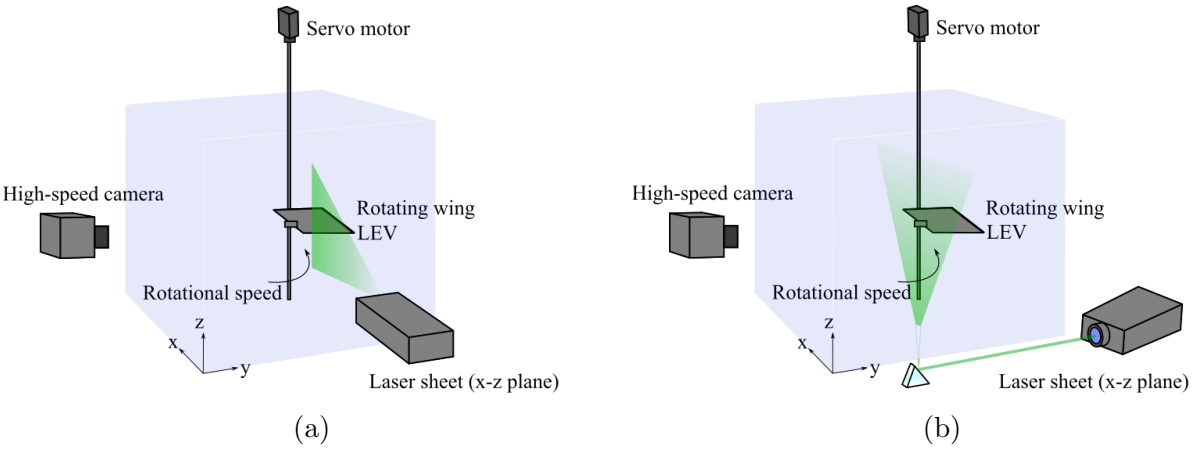

Figure 3.3: Experimental set-up for (a) the spanwise flow measurements (b) the LEV circulation growth measurements. In both cases, the laser sheet plane is parallel to the camera.

In order to determine the time-dependant LEV growth history and the shear-layer feeding velocity, the measurements are repeated at several wing revolution angles. The selected revolution angles vary from 90 degrees to 225 degrees with increments of 45 degrees, such that the impulsive start effects are excluded. Therefore, from hereonin, 'time' and 'azimuthal angle' will be used interchangeably.

A median normalization was performed prior to vector calculation in order to subtract the background image for each run and eliminate any systemic biases in illumination. Ten runs were recorded for each case. After the median normalization, only frames where the wing span and the camera's optical axis were aligned were retained to be processed.

Flow fields were calculated with a multi-grid/multi-pass cross-correlation algorithm. For each study case, an overlap of 50% was applied to the first two passes with the initial interrogation window and an overlap of 75% was applied to the last two passes. Asymmetric interrogation windows were utilized for the spanwise flow evaluation.

3.4 Results and Discussion

The basic topology of the vortex structure is illustrated with the vorticity fields in Figure 3.4. In this figure, azimuthal angle is increasing in subsequent sub-figures from left-to-right. This particular temporal evolution of the vorticity distribution is at the 1/3 span position for the $Re = 1000$ case at azimuthal angles of 90, 135, 180 and 225 degrees. However, for the purpose of showing the qualitative vortex evolution, this case is representative of the others. While the vortex size here is seen to grow between the first two angles, it is also clear that the vortex growth rate is approaching zero with azimuthal angle.

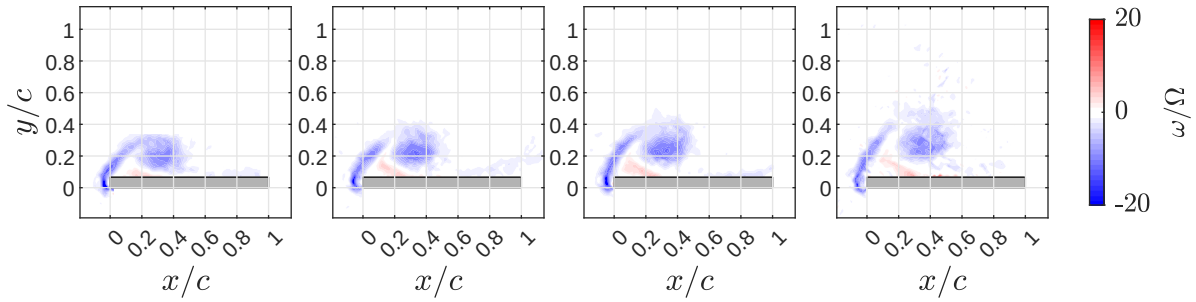

Figure 3.4: The normalized vorticity as a function of time for the spanwise position $z/Z_T = 1/3$ at $Re = 1000$

Meanwhile, Figure 3.5 shows the vorticity distribution instead as a function of span, at the same time for all subfigures (revolution angle of $\theta = 90$). As expected, the Figure shows that the LEV's area grows along the span from the most inboard position (1/4 of the span) to the most outboard position (1/2 of the span). Moreover, the vortex appears closer to the wing towards the wing root. Along the span, the vortex expands, both vertically and horizontally, leading to a displacement of the core further from the surface of the wing and the leading edge itself. Weaker secondary structures also appear in the shear layer in the far outboard positions. This pattern is the same at both Reynolds numbers and the LEV's area and vorticity magnitude for each position are comparable between both cases.

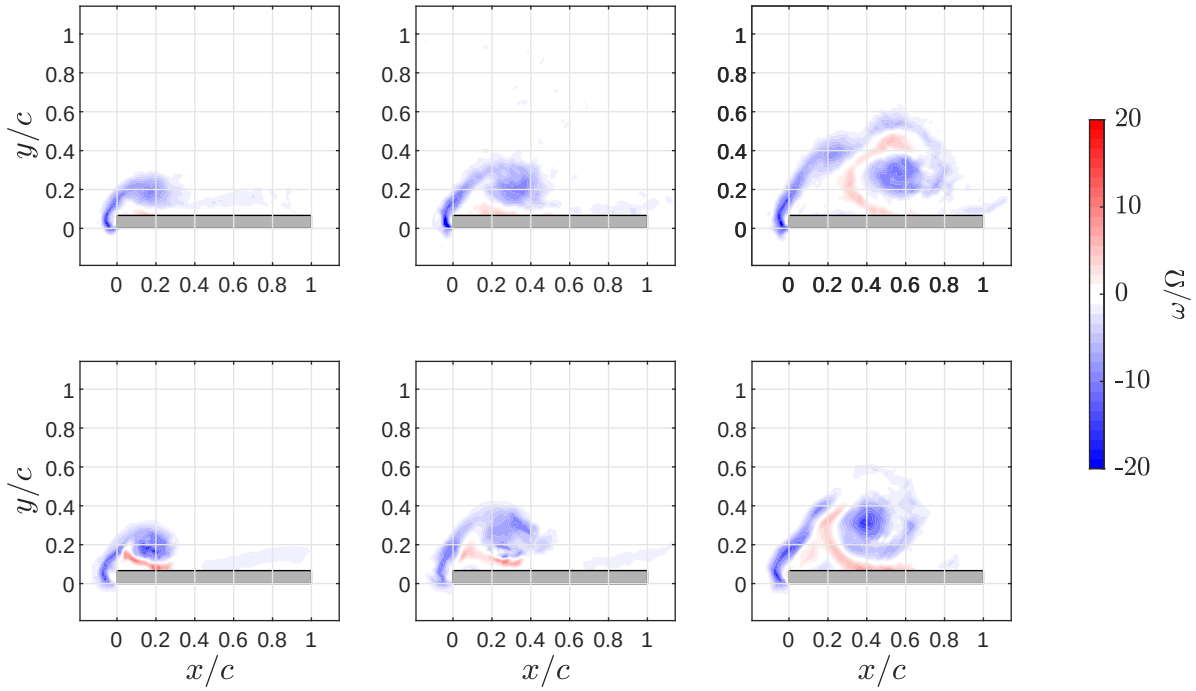

Figure 3.5: The normalized vorticity at the $z/Z_T = 1/4$, $1/3$ and $1/2$ positions for the $Re = 1000$ (upper row) and the $Re = 2500$ (lower row).

3.4.1 Vorticity Flux through the Shear-layer

The vortex feeding relationship proposed by Wong et al. (2018) was applied to a translating delta wing in that study, simplifying the process for evaluating the shear-layer feeding velocity. However, as the derivative model is applied here to a rotating wing, the same approximations no longer apply, and shear-layer properties are instead extracted directly from PIV data. It is therefore worth revisiting the approximation for shear-layer flux presented in Equation (3.3). As presented in Section 1, the model gives circulation flux as:

$$\frac{\partial \Gamma}{\partial t} = \frac{1}{2} u_o^2 \ . \tag{3.8}$$

The shear-layer velocity u_0 can be seen in Figure 3.6 as the peaks in velocity seen around $\eta = 0.8$. This can be compared to a direct measurement of vorticity flux from the same shear-layer data:

$$\left(\frac{\partial \Gamma}{\partial t}\right)_{\text{in}} = \int u\omega \mathrm{d}\eta = \int u \frac{\partial u}{\partial \eta} \mathrm{d}\eta \ , \tag{3.9}$$

where η is the shear-layer coordinate as presented in Figure 3.1, and u here is normal to this coordinate in both above equations. Figure 3.6 shows the velocity profile within the shear layer of the LEV along the span. The variation between Equations (3.8) and (3.9), was of the order of 5% for each test case. While either estimate will be sufficient for the exercise in the current work, this comparison suggests that this approximation for shear-layer flux remains robust for rotating wings.

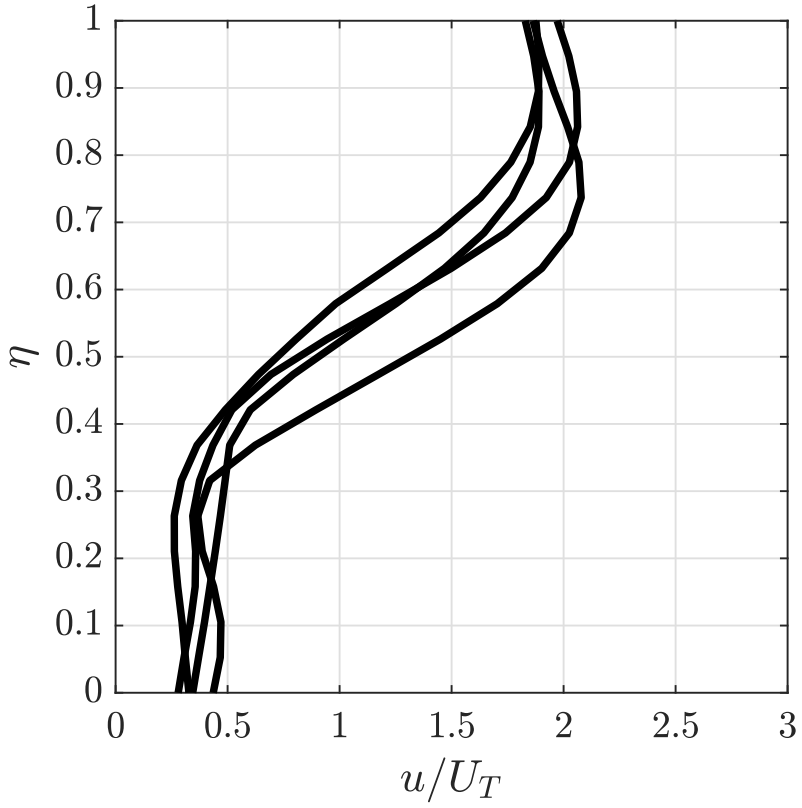

Figure 3.6: Representative velocity profiles within the shear layer of the LEV several individual cases (spanwise locations and azimuthal angles).Each curve was extracted from the average velocity field for that test case.

Therefore, the shear-layer velocity was measured along the span for both Reynolds number test cases, and for the purpose of feeding data into the semi-empirical model, intermediate

values were extracted from an interpolant. Furthermore, it was found that the normalized shear-layer velocities did not vary significantly with Reynolds number, to the extent that a single linear curve fit could conceivably capture both cases with minimal reduction in resolution. There was little time-dependency in the shear-layer velocity, such that shear-layer velocity was essentially fully determined by spanwise position.

3.4.2 Spanwise Flow

As discussed in Section 3.1.2, vorticity transport is mediated by spanwise flow. While the model from Maxworthy (2007) provides significant insight into the internal dynamics of spanwise flow in an LEV, it cannot be used as a predictive model without significant additional modelling effort. Specifically, the model developed by Maxworthy (2007) depends on the spanwise distribution of vortex area, whereas both shear-layer flux models and point vortex models tend to determine circulation independent of area. To convert between the two requires the vorticity distribution, at which point the relative cost and value of a CFD solution, for example, may be similar. Moreover, modelling vortex area requires knowledge of the vortex stretching throughout the domain. However, taking the work of Maxworthy (2007) in contrast with Van Den Berg and Ellington (1997), it is clear that there are competing factors determining spanwise flow. Here, Bernoulli's equation in rotating coordinates is used to produce a rough estimate of the relative importance of the spanwise pressure gradient versus rotational accelerations, and as a means to constrain the eventual curve fit of spanwise flow values that will eventually be used with the semi-empirical model.

Bernoulli's equation in rotating coordinates can be given as:

$$\frac{P}{\rho} + \frac{1}{2}\, w^2 - \frac{1}{2}\, z^2\, \Omega^2 = \text{const} \ , \tag{3.10}$$

where P represents the local pressure and Ω is the rate of rotation as mentioned previously. Limacher et al. (2016) derived an expression for the spanwise pressure gradient on a rotating wing, and found it to be proportional to radial location. Applying this yields:

$$w^2 = \frac{2\,k}{\rho}\frac{dP}{dz}\,z + \Omega^2 z^2 \ , \tag{3.11}$$

where k is an unknown constant of proportionality. This expression provides a physically-informed constraint on curve-fitting, while providing a physical interpretation of the resulting curve. The spanwise flow, as measured with PIV, is shown along with a fit version of Equation (3.11).

As seen in Figure 3.7 the spanwise flow variation along the span is well represented by a second degree polynomial, such as Equation (3.11). The spanwise flow values are similar at both Reynolds numbers. For both Reynolds numbers, the fitted value for Ω^2 is over an order of magnitude greater than $\frac{2}{\rho}\frac{k}{dz}\frac{dP}{dz}$, the pressure term accounting for less than 5% of the total spanwise flow.

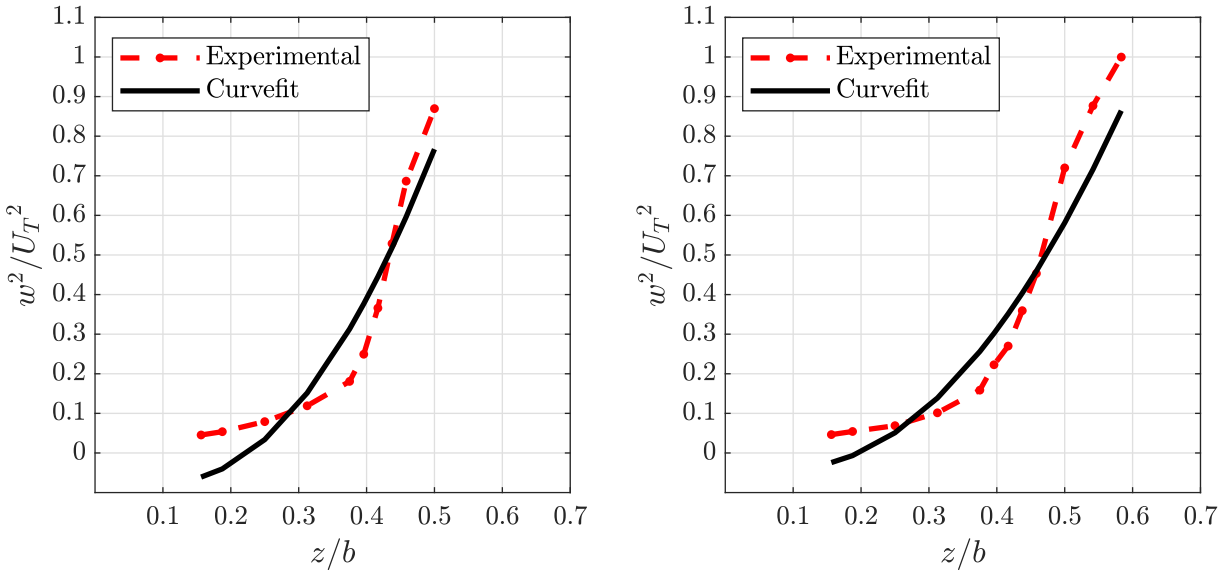

Figure 3.7: Curve fits of the spanwise flow when constrained to match the form suggested from Bernoulli's equation for (a) $Re = 1000$, and (b) $Re = 2500$. Spanwise flow is presented from 1/4 to 1/2 of the span. In both cases, spanwise flow is primarily driven by rotational acceleration rather than the pressure gradient.

For both Reynolds number cases, the curve fit produced estimates of rotational velocity Ω that are higher than the true physical value, and the Bernoulli inspired equation was

not expected to capture the complete physics. However, we hope that it does provide some insight for future efforts in modelling. For the purpose of this work, the analysis will not continue regarding the physics of the spanwise flow, and this model will simply be used as a curve fit.

Due to the sensitivity of the model on spanwise flow, circulation outputs derived from this curve fit are presented as a range, based on the 95% prediction interval of the fitting parameters. The curve fit itself was necessary, as velocities beyond the measurement domain were required for the model, and therefore the curve fit was used as an extrapolation function as well.

3.4.3 Circulation Transport

The primary hypothesis this work attempts to address is the role of vorticity annihilation on bulk circulation growth in an LEV. In this section, this hypothesis will be analysed by comparison of a real-world flow, versus a semi-empricial model constructed to eliminate all effects except for vorticity convection.

The circulation values predicted by the semi-empirical model are compared to the experimental circulation values in Figure 3.8. The experimental values are presented as broken lines while the modelled circulation values are presented as a shaded range, based on the 95% prediction interval for spanwise flow fitting parameters. Matching colors indicate spanwise position for easier visualisation. Following the thought-experiment presented in Section 3.4.2, circulation was computed in a rectangular control volume with one edge as close to the wing as possible for the measurement, rather than via a vortex identification criterion.

Vorticity annihilation, if it affects the bulk circulation values, would serve to reduce circulation, and therefore the model would be expected to over-estimate circulation. However, Figure 3.8 shows that the semi-empirical model, outlined in Section 2, and given appropriate outer shear-layer velocities and spanwise flow, accurately predicts the circulation of an LEV on a rotating wing, for each studied spanwise position and for both Reynolds numbers. As the semi-empirical model only considered circulation entering the LEV from the leading-edge

shear layer, and circulation leaving the LEV from spanwise convection, this result suggests that either there are no other significant terms within the circulation budget, or that these effects are local, and depend on the selection of control volume. While the 1/3 span position and the 1/4 span position for the $Re = 1000$ case are slightly above the modelled values, it is difficult to assign a systemic variation across all positions and cases, and, moreover, this is the opposite trend we would expect from vorticity annihilation. Therefore, at least in the kinematics tested here, the study concludes that many of the effects of vorticity annihilation on the bulk circulation value can be accounted by control volume selection.

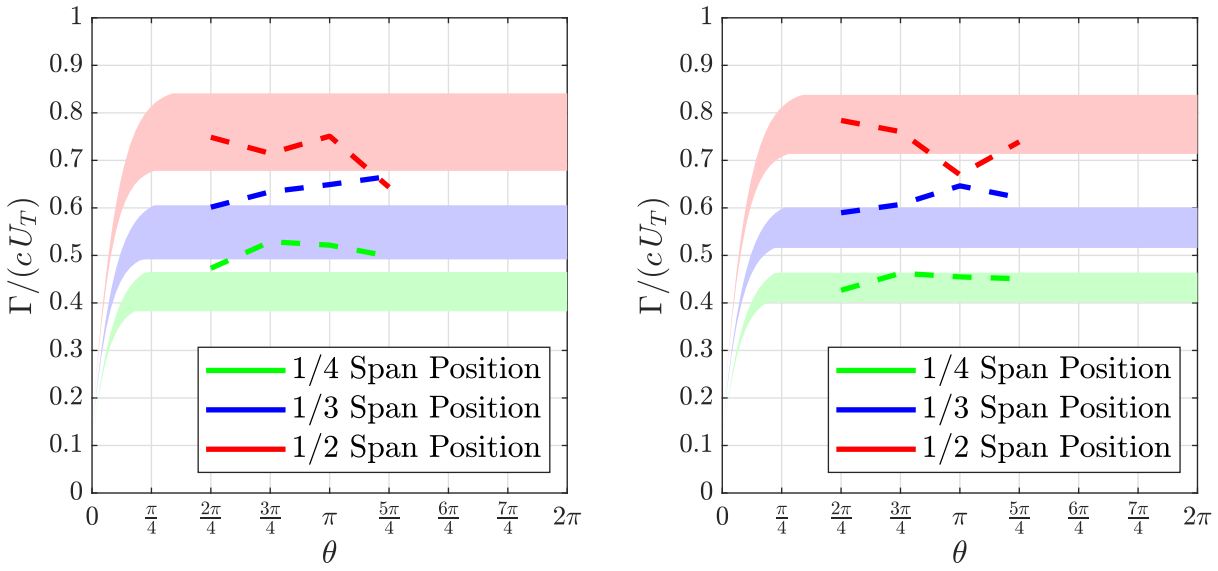

Figure 3.8: Circulation versus time for both experimental values (broken lines) and the values predicted by the semi-empirical model (shaded areas) for (a) $Re = 1000$, and (b) $Re = 2500$. Matching colors identify each spanwise location. Shaded areas represent the 95% prediction interval in the spanwise flow fitting parameters.

The circulation values are relatively insensitive to Reynolds number, which is consistent with Baik et al. (2012) who found that the Reynolds number effects in the two-dimensional vortex dynamics of an LEV are small. Later, Garmann et al. (2013) showed Reynolds number insensitivity to vortex topology in three dimensions as well. Therefore, we similarily conclude that viscous effects have only a minor effect if at all on the circulation budget, again given

appropriate control volume selection.

3.5 Conclusion

The present work aimed to investigate into the vorticity dynamics leading to the formation of a stable LEV on a rotating wing. In particular, the study aimed to determine the relative influence of vorticity annihilation on the bulk circulation of an LEV, as opposed to local effects.

A previous model describing the circulation of translating wings was adapted, based on the approximation of circulation transport as species transport tied to mass in the flow. As the model was adapted from translating wing at a much higher Reynolds number, a separate evaluation was made to validate the shear-layer feeding approximation, which was found to be met satisfactorily.

These assumptions were tested by comparing the circulation values predicted against experimental values. The experimental and modelled circulation values matched reasonably well, which is consistent with the hypothesis that the effect of the vorticity annihilation term on bulk circulation is small for these kinematics if the control volume includes the wing surface. Moreover, the lack of variation with Reynolds number suggests that the annihilation term, if present, is not a strong function of Reynolds number within this range. Indeed, the small difference between the experimental values and the model suggest that in some limited cases, circulation transport is adequately modelled as simple species transport. The present work suggests that, with respect to estimating total circulation, expanding the control volume may be sufficient to account for entrainment of opposite-sign vorticity from near the wing surface.

Chapter 4

Conclusion

The main purpose of the present work was to offer a model as an effective solution to predict the circulation distribution in a LEV for certain cases of highly three-dimensional flows. The modelling exercise presents itself by the definition of the circulation and the circulation transport. The model was developped and tested against experimental circulation measurements from flow fields measured via PIV on a fixed rotating wing in a 1 m^3 tank filled with water. The modelling exercise focused on the specific case of a strong and constant LEV, such that the flow is steady, on a rotating wing represented as a thin flat plate maintained under a low Reynolds numbers range varying from $Re = 1000$ to $Re = 2500$. While studying the net circulation, the study also limited its region of interest to strictly the primary vortex structures. While this study case is fairly specific, the modelling concepts explored and investigated are far reaching, and may be applied to many different test cases, such as the previously tested translating wing case. The positive outcomes resulting from the model concept for both the translating wing and the rotating wing is promising from a bio-engineered point of view, meaning research is a step closer to modelling (and understanding) the physics governing the circulation around a flapping wing.

While the outcome in itself is of value unto itself, as the model can offer accurate circulation predictions, the investigation also provided insight into fundamental fluid dynamics. As the model's circulation predictions match the experimental circulation measurements, it indicates that the model's characteristic governing equation (i.e. the vorticity transport

equation in its simplified form) is correct, and so are the assumptions made to define its simplified form. Therefore, the present work has established the role of each term characterizing the vorticity transport equation for an LEV in transcient flow leading to a stable vortex (i.e. vortex tilting, vortex stretching, viscous diffusion and vorticity annihilation) and their effects on the circulation generation and its transport in the case of a rotating wing.

4.1 Modelling Circulation

The suggested model conceptualizes the vorticity transport equation as species transport, such that circulation follows the mass (i.e. the fluid particles) in the flow. The total mass or circulation at a spanwise location is evaluated as the sum of all the particles at that location, which includes the particles generated that time-step and those previously generated and advected to that location. To develop the vorticity transport equation for steady flows into its species transport form, which is defined by a balance of the circulation generation rate and its transport through convection, the modelling exercise assumed the vortex stretching and the vortex tilting terms are negligible and disappear under integration or, at least, their effects are not significant when compared to convection. Additionally, the viscous diffusion term was assumed to be small enough to be ignored as its timescale is larger when compared to the vortex growth itself. As the circulation distribution predicted by the model matches the experimental circulation values, the model concept and, thus, its core assumptions were validated.

Moreover, the study demonstrated the viscosity has little effect on the circulation distribution. To show this, the study presented two test cases characterized by two different Reynolds numbers, selected as low values to maximise the viscous effects, if any. The similarity between the two test cases indicates the circulation distribution is insensitive to the Reynolds number variation, which confirm the viscous diffusion can be ignored for modelling purposes.

As the suggested model is conceptualized on circulation budget, an investigation on the vorticity annihilation mechanism effects on the net circulation was possible. As expected,

the investigation demonstrated that the vorticity annihilation mechanism doesn't need to be modelled when the selected control volume includes the entire LEV region (both positive and negative vorticity generated by primary and secondary vortices), such that it defines the net circulation. The predicted circulation values match experimental circulation values, validating that modelling net circulation is sufficient and accounts for the local effects of vorticity annihilation, without requiring an extra term to represent the vorticity annihilation.

4.2 Circulation Generation Conclusions

After validating the model concept and, thus, successfully modelling the circulation flux through the leading-edge shear layer, the study pushed its modelling exercise further and modelled the shear-layer velocity profile, which is a critical parameter in the circulation flux relationship developed. To do so, the study tested the applicability of a technique inspired by previous work in which the shear-layer velocity profile is defined by the acceleration of the flow around the blockage effect representative of the LEV. The relationships between the shear-layer velocity, the vortex area radius and the resulting mass entering the leading-edge was initially developed for a translating wing (e.g., Wong et al., 2013; Jia et al., 2021) but proved to give a good approximation for a rotating wing as well. As expected, this technique works with the species transport model developed, as the circulation entering the LEV shear-layer is represented with mass-containing vorticity fluid particles, meaning it is an easy addition to the initial model.

The modelled shear-layer velocity distribution overall proved to be a good approximation since it was in good agreement with the experimental shear-layer velocity extracted directly from experimental velocity fields. It is important to indicate that from the modelling exercise (the development of the model led to varying the controlling parameters), the suggested model proved to be less sensitive to shear-layer velocities than to spanwise flow values.

4.3 Circulation Transport Conclusions

The curvefit obtained from experimental spanwise flow measurements was, as expected, in close agreement for a significant fraction of with the second degree polynomial curve resultant from the w versus z plot, inspired from the modified Bernoulli equation for rotating coordinates. Furthermore, the rotational acceleration and the pressure gradient coefficients extracted from the curvefit confirmed the initial assumption which stated the pressure gradient is expected to be negligible in the case of a rotating wing. Indeed, the magnitude of the pressure gradient term represented less than $< 5\%$ of the total rotational acceleration term.

Thus, the spanwise flow distribution was approximated simply considering the rotational component, which was characterized by the physical rotational speed of the wing, such that the role of the circulation transport and its effects on the circulation growth were investigated. When compared to the experimental spanwise flow measurements the spanwise flow distribution predicted by the approximation appear to be initially a good fit, but deviate from the experimental data with increased span. While this indicate that the approximation isn't completely satisfying in itself to describe the spanwise flow distribution, the general goal is to define the circulation distribution, such that this disagreement still offer insights on the role of spanwise flow and the effects of circulation transport on circulation distribution. The predicted circulation values were in good agreement when spanwise flow was estimated most-accurately, which demonstrates that the circulation transport depends directly on spanwise flow. The underestimation of the circulation transport, or circulation removal, resulted in overestimation of circulation by the model.

4.4 Future work

Like much research, the current work provides both answers as well as new questions. One next step would be to implement and modify the model concept such that it predicts the circulation distribution within an LEV on a flapping wing. The circulation distribution

within the LEV on a flapping wing is important to fluid mechanisms of biological swimming and flying research as it is identified as one of the high lift mechanism, meaning it defines both lift generation and flight control. Therefore, modelling the circulation distribution around a flapping wing, which may require understanding of the controlling parameters characterizing the wing kinematics, would lead to accurate aerodynamics forces predictions.

Since, the proposed model concept was tested and validated for both translating and rotating wing, it should apply to the circulation over flapping wings as well, since the flapping motion can be represented as a combination of the two. However, three-dimensional flows presents highly complex flow behaviours and dynamics characterized by intertwined relationships, such that the outcomes are hardly intuitive. An effective model to predicts the circulation distribution on a flapping wing would lead to tremendous improvements for the bio-inspired and bio-engineered flights, which is beneficial for MAVs and UAVs designs.

Bibliography

Y. S. Baik, L. P. Bernal, K. Granlund, and M. V. Ol. Unsteady force generation and vortex dynamics of pitching and plunging aerofoils. *Journal of Fluid Mechanics*, 709:37–68, 2012.

A. M. Berg and A. A. Biewener. Wing and body kinematics of takeoff and landing flight in the pigeon (Columba livia). *Journal of Experimental Biology*, 213(10):1651–1658, 2010.

J. M. Birch, W. B. Dickson, and M. H. Dickinson. Force production and flow structure of the leading edge vortex on flapping wings at high and low Reynolds numbers. *Journal of Experimental Biology*, 207(7):1063–1072, 2004.

A. C. Carruthers, A. L. Thomas, and G. K. Taylor. Automatic aeroelastic devices in the wings of a steppe eagle Aquila nipalensis. *Journal of Experimental Biology*, 210(23):4136–4149, 2007.

A. C. Carruthers, A. L. Thomas, S. M. Walker, and G. K. Taylor. Mechanics and aerodynamics of perching manoeuvres in a large bird of prey. *The Aeronautical Journal*, 114 (1161):673–680, 2010.

B. Cheng, S. P. Sane, G. Barbera, D. R. Troolin, T. Strand, and X. Deng. Three-dimensional flow visualization and vorticity dynamics in revolving wings. *Experiments in fluids*, 54(1): 1–12, 2013.

J. Deparday and K. Mulleners. Modeling the interplay between the shear layer and leading edge suction during dynamic stall. *Physics of Fluids*, 31(10):107104, 2019.

J. Deparday, X. He, J. D. Eldredge, K. Mulleners, and D. R. Williams. Experimental quantification of unsteady leading-edge flow separation. *Journal of Fluid Mechanics*, 941, 2022.

K. P. Dial. Avian forelimb muscles and nonsteady flight: can birds fly without using the muscles in their wings? *The Auk*, 109(4):874–885, 1992.

N. Didden. On the formation of vortex rings: rolling-up and production of circulation. *Zeitschrift für angewandte Mathematik und Physik ZAMP*, 30(1):101–116, 1979.

J. D. Eldredge and A. R. Jones. Leading-edge vortices: mechanics and modeling. *Annual Review of Fluid Mechanics*, 51:75–104, 2019.

C. P. Ellington, C. Van Den Berg, A. P. Willmott, and A. L. Thomas. Leading-edge vortices in insect flight. *Nature*, 384(6610):626–630, 1996.

D. J. Garmann, M. R. Visbal, and P. D. Orkwis. Three-dimensional flow structure and aerodynamic loading on a revolving wing. *Physics of Fluids*, 25:034101, 2013.

M. S. Hemati, J. D. Eldredge, and J. L. Speyer. Improving vortex models via optimal control theory. *Journal of Fluids and Structures*, 49:91–111, 2014.

K. Jia, T. Scofield, M. Wei, and S. Bhattacharya. Vorticity transfer in a leading-edge vortex due to controlled spanwise bending. *Physical Review Fluids*, 6(2):024703, 2021.

A. Jones and H. Babinsky. Reynolds number effects on leading edge vortex development on a waving wing. *Experiments in fluids*, 51(1):197–210, 2011.

A. Jones, C. P. Ford, and H. Babinsky. Three-dimensional effects on sliding and waving wings. *Journal of aircraft*, 48(2):633–644, 2011.

D. Lentink and M. H. Dickinson. Biofluiddynamic scaling of flapping, spinning and translating fins and wings. *Journal of Experimental Biology*, 212(16):2691–2704, 2009a.

D. Lentink and M. H. Dickinson. Rotational accelerations stabilize leading edge vortices on revolving fly wings. *Journal of Experimental Biology*, 212(16):2705–2719, 2009b.

E. Limacher, C. Morton, and D. Wood. On the trajectory of leading-edge vortices under the influence of Coriolis acceleration. *Journal of Fluid Mechanics*, 800, 2016.

F. Manar, A. Medina, and A. R. Jones. Tip vortex structure and aerodynamic loading on rotating wings in confined spaces. *Experiments in fluids*, 55(9):1–18, 2014.

T. Maxworthy. The formation and maintenance of a leading-edge vortex during the forward motion of an animal wing. *Journal of Fluid Mechanics*, 587:471–475, 2007.

A. Medina and A. R. Jones. Leading-edge vortex burst on a low-aspect-ratio rotating flat plate. *Physical Review Fluids*, 1(4):044501, 2016.

B. Morton. The generation and decay of vorticity. *Geophysical & Astrophysical Fluid Dynamics*, 28(3-4):277–308, 1984.

S. Narsipur, P. Hosangadi, A. Gopalarathnam, and J. R. Edwards. Variation of leading-edge suction during stall for unsteady aerofoil motions. *Journal of Fluid Mechanics*, 900, 2020.

K. Onoue and K. S. Breuer. A scaling for vortex formation on swept and unswept pitching wings. *Journal of Fluid Mechanics*, 832:697–720, 2017.

E. C. Polhamus. A concept of the vortex lift of sharp-edge delta wings based on a leading-edge-suction analogy. Technical report, 1966.

K. Ramesh, A. Gopalarathnam, K. Granlund, M. V. Ol, and J. R. Edwards. Discrete-vortex method with novel shedding criterion for unsteady aerofoil flows with intermittent leading-edge vortex shedding. *Journal of Fluid Mechanics*, 751:500–538, 2014.

K. Ramesh, K. Granlund, M. V. Ol, A. Gopalarathnam, and J. R. Edwards. Leading-edge flow criticality as a governing factor in leading-edge vortex initiation in unsteady airfoil flows. *Theoretical and Computational Fluid Dynamics*, 32(2):109–136, 2018.

D. E. Rival and C. Tropea. Characteristics of pitching and plunging airfoils under dynamic-stall conditions. *Journal of Aircraft*, 47(1):80–86, 2010.

D. E. Rival, T. Prangemeier, and C. Tropea. The influence of airfoil kinematics on the formation of leading-edge vortices in bio-inspired flight. pages 261–271. 2010.

D. E. Rival, J. Kriegseis, P. Schaub, A. Widmann, and C. Tropea. Characteristic length scales for vortex detachment on plunging profiles with varying leading-edge geometry. *Experiments in fluids*, 55(1):1–8, 2014.

A. Roshko. On the drag and shedding frequency of two-dimensional bluff bodies. Technical report, 1954.

B. Tobalske. Biomechanics of bird flight. *Journal of Experimental Biology*, 210(18):3135–3146, 2007.

B. Tobalske and K. Dial. Flight kinematics of black-billed magpies and pigeons over a wide range of speeds. *The journal of experimental biology*, 199(2):263–280, 1996.

B. W. Tobalske, D. L. Altshuler, and D. R. Powers. Take-off mechanics in hummingbirds (Trochilidae). *Journal of Experimental Biology*, 207(8):1345–1352, 2004.

C. Van Den Berg and C. P. Ellington. The three–dimensional leading–edge vortex of a 'hovering'model hawkmoth. *Philosophical Transactions of the Royal Society of London. Series B: Biological Sciences*, 352(1351):329–340, 1997.

C. J. Wojcik and J. H. Buchholz. Vorticity transport in the leading-edge vortex on a rotating blade. *Journal of Fluid Mechanics*, 743:249–261, 2014.

J. G. Wong and D. E. Rival. Determining the relative stability of leading-edge vortices on nominally two-dimensional flapping profiles. *Journal of Fluid Mechanics*, 766:611–625, 2015.

J. G. Wong, J. Kriegseis, and D. E. Rival. An investigation into vortex growth and stabilization for two-dimensional plunging and flapping plates with varying sweep. *Journal of Fluids and Structures*, 43:231–243, 2013.

J. G. Wong, G. Gillespie, and D. E. Rival. Circulation redistribution in leading-edge vortices with spanwise flow. *AIAA Journal*, 56(10):3857–3862, 2018.